JGR Biogeosciences

RESEARCH ARTICLE
10.1029/2022JG006943

Special Section:
Advances in scaling and modeling of land-atmosphere interactions

Methane and Carbon Dioxide Fluxes in a Temperate Tidal Salt Marsh: Comparisons Between Plot and Ecosystem Measurements

Andrew C. Hill[1] and **Rodrigo Vargas**[1]

[1]Department of Plant & Soil Sciences, University of Delaware, Newark, DE, USA

Key Points:

- Plot-level and eddy covariance measurements had good overall agreement, but the strength of agreement was dependent upon plant phenology
- The relevance and influence of environmental drivers varied for all fluxes across different techniques
- Models parameterized with plot-level data overestimated ecosystem-scale net ecosystem exchange but underestimated CO_2 and CH_4 emissions

Supporting Information:

Supporting Information may be found in the online version of this article.

Correspondence to:

R. Vargas,
rvargas@udel.edu

Citation:

Hill, A. C., & Vargas, R. (2022). Methane and carbon dioxide fluxes in a temperate tidal salt marsh: Comparisons between plot and ecosystem measurements. *Journal of Geophysical Research: Biogeosciences*, *127*, e2022JG006943. https://doi.org/10.1029/2022JG006943

Received 20 APR 2022
Accepted 28 JUN 2022

Author Contributions:

Conceptualization: Andrew C. Hill, Rodrigo Vargas
Formal analysis: Andrew C. Hill
Funding acquisition: Rodrigo Vargas
Investigation: Andrew C. Hill
Methodology: Andrew C. Hill, Rodrigo Vargas
Writing – review & editing: Andrew C. Hill, Rodrigo Vargas

Abstract

Tidal wetlands are comprised of complex interdependent pathways where measurements of carbon exchange are often scale dependent. Common data collection methods (i.e., chambers and eddy covariance) are inherently constrained to different spatial and temporal scales which could generate biased information for applications of carbon accounting, identifying functional relationships and predicting future responses to climate change. Consequently, it is needed to systematically evaluate measurements derived from multiple approaches to identify differences and how techniques complement each other to reconcile interpretations. To accomplish this, we tested ecosystem-scale eddy covariance with plot-scale chamber measurements within a temperate salt marsh. We found good agreement (R^2 = 0.71–0.95) when comparing measurements of CH_4 emissions and CO_2 exchange but this agreement was dependent upon canopy phenology with discrepancies mainly arising during senescence and dormancy phenophases. The environmental drivers for CH_4 and CO_2 fluxes were mostly preserved across different measurement techniques, but the number of drivers increases while their individual strength decreases at the ecosystem scale. Empirical upscaling models parameterized with chamber measurements overestimated annual net ecosystem exchange (NEE; 108%) and gross primary production (GPP; 12%) while underestimating ecosystem respiration (Reco; 14%) and CH_4 emissions (69%) compared to eddy covariance measurements. Our results suggest that the environmental complexity of CH_4 and CO_2 fluxes in salt marshes may be underestimated by chamber-based measurements, and highlights how different techniques are complementary while considering limitations at each level of measurement.

Plain Language Summary

Tidal wetlands are important landscape features which play a significant role in regional carbon cycling between land, ocean and the atmosphere. These ecosystems are very productive, with high rates of photosynthesis during the growing season, but they also emit methane and carbon dioxide which can offset carbon gains. Therefore, it is important to accurately measure and understand what factors regulate carbon cycling processes to better characterize how these systems function, calculate carbon budgets and help predict possible reposes to climate change. We compare several common measurement techniques including chamber and eddy covariance which incorporate information across different scales to evaluate the level of agreement and how these techniques can be combined to increase our understanding of ecosystem functionality. We found that techniques agree well when comparing time-matched measurement windows but different plant development stages across the ecosystem likely impacted agreement during autumn and early winter. We found that primary factors regulating fluxes were similar across techniques but when considering data collected over more hours of the day with eddy covariance, additional factors were identified indicating measurements from chambers which are limited in both coverage across space and time may present an oversimplified view within tidal wetlands.

1. Introduction

Tidal wetlands occupy a fraction of terrestrial land cover yet play an important role in global carbon cycling by serving as regional biogeochemical hotspots. The high magnitude of net primary productivity and positioning at the terrestrial-aquatic interface supports open transfers and transformation of energy and mass across system boundaries (Al-Haj & Fulweiler, 2020; Cai, 2011), while biogeochemical conditions of the sediments slows re-oxidation and vertical release of CH_4 and CO_2 (Alongi, 2020; Emery et al., 2021). These features have framed tidal wetlands as key systems for studying effects of changing environmental conditions and increased weather variability. As such, there has been a strong interest in reconciling information derived from different approaches

within these ecosystems (Feagin et al., 2020; Holmquist & Windham-Myers, 2022; Trifunovic et al., 2020; Wang et al., 2021), but there are still uncertainties that require further studies to clarify how different techniques and data streams can be utilized for carbon accounting/budgeting purposes, system characterization and improved forecasting capabilities as a result of climate change.

Multiple approaches exist to measure CH_4 and CO_2 fluxes to the atmosphere and the chamber based method has been widely used across a wide range of ecosystems (Oertel et al., 2016). This method is well suited for factorial studies where control and experimental plots can easily be distinguished from background noise of the ecosystem or for survey approaches to capture spatial heterogeneity (Czapla et al., 2020b; Villa et al., 2021). Chambers can also be used to acquire direct measurements of respiration, thus better constraining ecosystem respiration (Reco) and gross primary productivity (GPP) estimates from other approaches (Reichstein et al., 2012; Stoy et al., 2006). However, when applied for carbon accounting or modeling, infrequent sampling could present challenges for proper system representation and identifying functional relationships (Cueva et al., 2017). These concerns may be especially relevant for salt marshes where a dynamic range of biogeochemical conditions are modulated by common drivers for wetlands such as light, water level and temperature (Capooci & Vargas, 2022; Huertas et al., 2019; Vazquez-Lule & Vargas, 2021), but also tidal activity and salinity. Furthermore, chambers can only represent a small area (i.e., footprint) of the landscape, capture snapshots in time, and therefore may fail to capture emergent ecosystem properties that can manifest over larger spatial and temporal scales.

As an alternative and more modern approach, the eddy covariance technique (EC) allows for near-continuous measurements of mass and energy exchange at ecosystem-scale (Forbrich & Giblin, 2015; Kathilankal et al., 2008; Vazquez-Lule & Vargas, 2021). When paired with temporally aligned ancillary data (e.g., water level, meteorological variables), EC can provide detailed information about ecosystem functionality (Li et al., 2018; Wei et al., 2020). This technique is not without errors, and there are several challenges including loss of data during low turbulence, maintenance requirements, high start-up cost and dedicated site infrastructure which could impose limitations. More importantly, EC cannot directly resolve which land cover fractions (i.e., soils, plants, and standing water) are contributing to the overall fluxes as measurements are integrated in respect to both time and space to capture high and low frequency flows (Moncrieff et al., 2005). Additionally, fluxes of GPP and Reco are estimated as a result of a model based on temperature or light (Lasslop et al., 2012; Reichstein et al., 2005), and are not directly measured which introduces additional uncertainties. While both chambers and EC based approaches have their own benefits and limitations, the paired use of methods can be an especially powerful tool for reconciling differences between approaches (Barba et al., 2021; Fox et al., 2008). Specifically, including a data subset with higher spatiotemporal integration from EC (i.e., daily averaged data) can serve as a target benchmark to compare other methods, thus helping to bridge the gap between different measurement scales (e.g., plot-ecosystem) (Hill, Barba, et al., 2021; Lucas-Moffat et al., 2018).

Most studies that have made efforts to address differences between EC and chamber measurements have been based within terrestrial ecosystems. These efforts have mainly focused on soil respiration and typically report higher emissions from chambers in comparison with EC measurements (e.g., Barba et al., 2018; Janssens et al., 2000), as attributed to uncertainties in the calculation of ecosystem-scale respiration and limitations in spatial coverage of chamber measurements (Barba et al., 2018; Phillips et al., 2017). Findings are mixed for CH_4 fluxes with studies reporting higher emissions from chambers (Hendriks et al., 2010; Yu et al., 2013) but also higher emissions from EC (Chaichana et al., 2018; Forbrich et al., 2011; You et al., 2021). There are fewer studies which have included GPP and Reco by utilizing opaque and transparent chambers (Lucas-Moffat et al., 2018; Poyda et al., 2017; Riederer et al., 2014). Many of these studies report good agreement when aligning time averaged measurements, yet greater discrepancies or systematic offsets can occur when upscaling or extrapolating measurements to an annual period (Hendriks et al., 2010; Lucas-Moffat et al., 2018; Morin et al., 2017; Wang et al., 2010). While salt marshes are typically homogeneous in vegetation coverage, they are also dynamic, difficult to access and measure, and it is unclear how these measurements differ and complement each other.

The current study explores measurements of CH_4 and CO_2 fluxes from plots (i.e., vegetation + sediments), vegetation, sediments and at the ecosystem scale within a temperate tidal salt marsh. A combination of measurement techniques which integrate information at different spatial scales are used to examine component fluxes of CH_4 emissions, NEE, GPP and Reco. We use temporally aligned data to generate representative time periods from EC data to evaluate the level of real-time synchronicity, examine functional relationships to explore driver

importance across different measurement techniques and apply empirical upscaling to compare chamber- and EC-derived carbon budgets.

We postulate three interrelated hypotheses: We expect an overall good agreement between plot and ecosystem-scale carbon fluxes (H1), as plots are located within a representative area of the EC footprint consisting of homogeneous land cover, but we also expect large uncertainty imposed by tidal cycles and salinity changes. Previous studies examining CO_2 exchange in peatlands (Heikkinen et al., 2002; Lees et al., 2021) and a reed marsh (Acosta et al., 2019) reported lower fluxes from chambers, while studies examining CH_4 emissions have found higher fluxes from chambers in a variety of different wetlands (Chaichana et al., 2018; Hendriks et al., 2010; Meijide et al., 2011; Sun et al., 2013). Only two previous studies have performed similar comparisons in a salt marsh where CH_4 and CO_2 emissions from chambers were found to be 2 times higher than ecosystem-scale fluxes (Krauss et al., 2016), and NEE derived from chambers was of greater magnitude than ecosystem-scale fluxes (Czapla et al., 2020). We expect that functional relationships and environmental drivers will be preserved across techniques but the relative importance of each driver will be different (H2). The underlying assumptions of this hypothesis is critical for justifying the use of chamber-based measurements for model development and parameterization, but there is evidence that functional relationships may be influenced by different techniques in salt marshes (Capooci & Vargas, 2022). Finally, we postulate the null hypothesis that modeled annual fluxes and budgets from plot measurements will agree with measured (NEE, CH_4) and partitioned (GPP, Reco) rates from EC (H3). This study provides novelty by systematically combining and comparing flux measurement techniques which integrate information from different spatial scales within a tidal salt marsh.

2. Materials and Methods

2.1. Study Site

The study site is the St Jones Reserve (39.09°N, 75.44°W) which has been described extensively elsewhere (Hill, Vázquez-Lule, & Vargas, 2021; Vazquez-Lule & Vargas, 2021). Briefly, the site represents a temperate salt marsh located along the Delaware Bay, with a mean elevation of 0.60 ± 0.26 m relative to NAVD88 datum (McKenna et al., 2018). Vegetation is dominated by a monoculture of short form *Spartina alterniflora* L. (saltmarsh cordgrass; recently referred to as *Sporobolus alterniflorus*; Peterson et al., 2014), with patches of tall *S. alterniflora*, *S. cynosuroides* and *P. australis* along creek banks. The site is mesohaline and during the year 2020 the average salinity was 8.43 ppt with a range of 0.2–25.0 ppt at the tidal creek. Climate is humid subtropical (Cfa) with a 2020 annual average air temperature and total annual precipitation of 14.1°C and 717.0 mm, respectively. The site is part of the AmeriFlux, Phenocam, and SpectNet networks (Site ID: US-StJ), as well as part of NOAA's National Estuarine Research Reserve System.

2.2. Plot-Scale CO_2 and CH_4 Measurements

Five 1 m^2 plots were established to perform manual flux measurements across a representative stand of short form *Spartina alternifloria* L. within the footprint of an eddy covariance tower. We utilized two types of plot-scale chamber designs: (a) semi-transparent cover (90% PAR transmission); and (b) opaque cover (i.e., dark chamber). These chambers incorporate both the sediment and overlying plant canopy within each plot. The frames of the chambers were constructed of polyvinyl chloride (PVC) piping and 6 mm polyethylene; chamber bottoms were fitted with a 19 mm high density neoprene compressible rubber gasket. Measurements from the semi-transparent chambers represent plot-scale NEE; dark chambers represent plot-scale Reco; and the difference between consecutive semi-transparent and dark measurements (i.e., NEE minus Reco) on the same plot represent plot-scale GPP. CH_4 fluxes were recorded concurrently with NEE measurements using semi-transparent chambers. Similar chambers are commonly used for greenhouse gas flux measurements to study land-atmosphere interaction (Limmer et al., 2018; Poyda et al., 2017; Tong et al., 2010).

These chamber measurements were taken using a closed loop sampling design with chamber air circulated through an ultra-portable greenhouse gas analyzer (LGR; Los Gatos Research, Model 915-0011, San Jose, CA) capable of reading both CH_4 and CO_2 (Limmer et al., 2018). A small fan was used to mix chamber air and closure time was approximately 3 min per frame. To reduce any carry-over impacts from the prior chamber measurement, we first sampled all five plots consecutively with semi-transparent chambers, followed by dark chambers. Measurement sets across plots spanned 30 min under clear sky conditions to reduce as much as possible variation

in environmental conditions between sets. Sampling campaigns for all measurements were performed twice monthly (approx. 7 days apart) from May to December to capture a variety of conditions including opposing tidal stages (high vs. low water level) and seasonal (phenology) differences. Fluxes were calculated from LGR raw data using either linear or exponential curve fits based on chamber concentration increase during closure time (Pearson et al., 2016; Warner et al., 2018).

We removed any cases where the regressions used for estimating fluxes displayed an $R^2 < 0.90$ (primarily associated with chamber disturbance), with the exception of dormancy measurements where concentration increases were near zero. In these cases, we adjusted our QA/QC criteria to avoid removal of any flux falling within ±0.20 standard deviations of the mean flux (±0.99 μmol CO_2 m^{-2} s^{-1}) (Hill, Barba, et al., 2021). If the QA/QC test was sufficient for CO_2 we made the assumption that micrometeorological conditions of chambers were also valid for CH_4 fluxes (Barba et al., 2021; Capooci et al., 2019). For any given measurement day, we used the average of all five plots and included the standard deviation as a metric of spatial variability across chambers. While we did not explicitly test the contributions from different emissions pathways (diffusion vs. ebullution), yet we made extensive efforts to eliminate any physical disturbances (via elevated boardwalks, gentle chamber placement) which could result in artificially forced emission spikes. Natural bubble release processes still likely occurred periodically but the relatively large well-mixed chambers help provide buffering on sudden concentration changes.

2.3. Leaf-Scale and Sediment Measurements

Measurements of net carbon uptake were measured at leaf-scale using the leaf-cuvette of a portable photosynthesis analyzer (Li-6400, Licor, Lincoln, NE). Measurements were taken just prior to plot-scale chamber measurements on two separate representative plants located adjacent to each plot (10 plants sampled each campaign). Since we were interested in observing fluxes occurring under current "real-time" conditions, readings were performed survey style and the cuvette environment was adjusted to match ambient conditions (incident radiation, CO_2, humidity) with a flow rate of 500 μmol s^{-1}. Readings were logged after CO_2 stabilization with an average closure time of 1 min (Hill et al., 2019). Photosynthesis rates were recorded per unit leaf area (as reported by the instrument), but we scaled measurements to plot ground area (1 m^2) for cross comparisons by multiplying fluxes by the leaf area index (LAI) of each plot as measured from an Accupar LP-80 ceptometer (Meter Inc, Pullman, WA, USA).

Within the bounds of each 1 m^2 plot we installed two (18 cm diameter) PVC sediment collars and used a small opaque closed chamber with an LGR analyzer to measure sediment-atmosphere CH_4 and CO_2 emissions. Total area occupied by the collars was 5.1% of each 1 m^2 plot footprint. Vegetation was excluded within these collars by clipping at the sediment surface which was maintained throughout the study period. Sediment chamber closure time was approximately 2 min and QA/QC procedures were the same as for plot chambers (Capooci & Vargas, 2022).

2.4. Ecosystem-Scale Eddy Covariance Measurements

The eddy covariance technique (Aubinet et al., 2012; Baldocchi, 2003) was used to provide ecosystem-scale measurements on the net exchange of CH_4 and CO_2. Gas concentration and wind data was collected at 10 Hz from an enclosed path CO_2/H_2O infrared gas analyzer (Li-7200, Licor, Lincoln, NE, USA), open path CH_4 analyzer (Li-7700, Licor, Lincoln, NE, USA) and 3D sonic anemometer (Gill Windmaster Pro, Gill Instruments, Lymingtonm, UK). The instruments were located approximately 110 m SW of the plots. While specific details on tower set-up and pre-processing can be found elsewhere (Vazquez-Lule & Vargas, 2021), we used Eddy Pro software (version 7.0.6) to perform time lag compensation, double coordinate rotation on wind components and Reynold's block averaging to obtain flux data at 30 min intervals. We applied several modified Ameriflux processing steps including filtering of flagged QA/QC values, removal of CO_2 flux outliers (−50 to 50 μmol m^{-2} s^{-1}), incorporation of nighttime storage fluxes and footprint filtering based on Kormann and Meixner (2001) and physical marsh boundaries along the upland terminus. Outliers from CH_4 data were retained as large pulses of CH_4 are possible during ebullition or hydrologically mediated events (Li et al., 2018). Together, this removed 27% and 23% of half-hourly fluxes for CH_4 and CO_2, respectively. Gap filling of CH_4 and CO_2 was performed using marginal distribution sampling (MDS) moving look-up tables utilizing variables of latent energy (LE), sensible heat (H), net radiation (Rg), soil temperature (Tsoil), air temperature (Tair) and relative humidity (rH) for CO_2 data and

Tsoil, Tair, water level and dissolved oxygen (DO) for CH_4 data (Vazquez-Lule & Vargas, 2021). Partitioning of GPP and Reco from net CO_2 exchange (NEE) (i.e., nighttime method, Reichstein et al., 2005) was performed using the REddyProc R package (Reichstein et al., 2005; Wutzler et al., 2018). For comparisons between eddy covariance and chamber measurements we did not include gap filled data. We only included gap filled data for calculating annual sums and daily means for statistical models.

2.5. Ancillary Data

Meteorological data was acquired from an on-site station located approximately 80 m from the eddy covariance tower. Data was collected for air temperature (Tair) and humidity (HC2-S3, Campbell Scientific, Logan, UT), pressure (Patm) (CS-106, Vaisala, Vantaa, Finland), precipitation (ppt) (TE 525, Tipping Bucket Rain Gauge, Campbell Scientific, Logan, UT) and photosynthetically active radiation (PAR) (SQ-110, quantum sensor, Apogee, Logan, UT). Water quality data was acquired from the main tidal creek which runs adjacent to the eddy covariance tower (10 m). Data was collected for water temperature (Twater), salinity (Sal), dissolved oxygen (DO) and depth (level) from a YSI EXO2 sonde outfitted with EXO sensors. We also included information on soil temperature (Tsoil) collected from a separate instrument station located 20 m from plots. The collection of meteorological and water quality data follows the National Estuarine Research Reserve's Centralized Data Management Protocol (Kennish, 2019). Meteorological data can be accessed via the National Estuarine Research Reserve System's Centralized Data Management Office (NERR CDMO; station: delsjmet-p).

2.6. Statistical Analysis

2.6.1. Representative Time Period Comparisons

We calculated representative time periods with 3.5 hr subsets of EC data (i.e., from 7 half-hour measurements) to compare differences between measurement techniques. Vegetation and sediment-atmosphere fluxes, which required less measurement time, were compared using a representative time period of 1.5 hr of EC data (i.e., calculated from 3 half-hour measurements). To organize measurement techniques and the data generated from each, we applied a naming convention where $Plot_{exp}$, $Leaf_{exp}$, $Sediment_{exp}$ and EC_{exp}, are the collective measurement sets from plot chambers, plot vegetation, sediment chambers and the representative eddy covariance time periods, respectively. The means from these subsets were compared with either a Welch's *t*-test or a Wilcox signed-rank test dependent upon normality confirmation (Shapiro-Wilks). The plot subsets ($Plot_{exp}$, $Leaf_{exp}$, $Sediment_{exp}$) were also compared to the ecosystem subset (EC_{exp}) by linear regression to ascertain cross-scale relationships.

2.6.2. Functional Relationships and Statistical Modeling

To determine the strength of key functional relationships across measurement techniques, we first took a standardized approach and assembled simple regression models. All variables which were selected for the subsequent multivariate models were used to test bivariate relationships (linear vs. exponential) at each measurement level ($Plot_{exp}$, $Leaf_{exp}$, $Sediment_{exp}$, EC_{exp} and EC_{dd}) for each relevant flux component (NEE, GPP, Reco and CH_4).

To explore driver importance more thoroughly, we then took a multivariate approach by assembling generalized least squares (GLS) statistical models at each measurement level ($Plot_{exp}$, $Leaf_{exp}$, $Sediment_{exp}$, EC_{exp} and EC_{dd}). We also added a higher hierarchical level of data consisting of daily daytime averaged EC measurements (EC_{dd}), covering the period chambers were deployed (May to December, $n = 244$) to represent a more complete time-integrated system. Models were generated for each flux component to obtain relevant drivers and response strengths (*nlme* R package; Pinheiro et al., 2017). Independent variable distributions were inspected for normality (Shapiro-Wilks) and skewness (moments *R* package; Komsta & Novomestky, 2015). Log and square-root transformations were performed on CH_4 and CO_2 emissions to adjust for right-skewed data. If the transformation generated negative values (as with Reco), a constant was added prior to transforming to set all values positive. All potential driver variables were scaled by setting a zero mean with a one unit standard deviation to allow cross model coefficient comparison. Temporal autocorrelations were accounted for between concurrent days or measurement sets (approx. 7 days apart).

We initially considered all ancillary drivers including full meteorology and water quality data. Saturated models were inspected for variance inflation factor (VIF) and any variable with a VIF >3 was removed from the analysis.

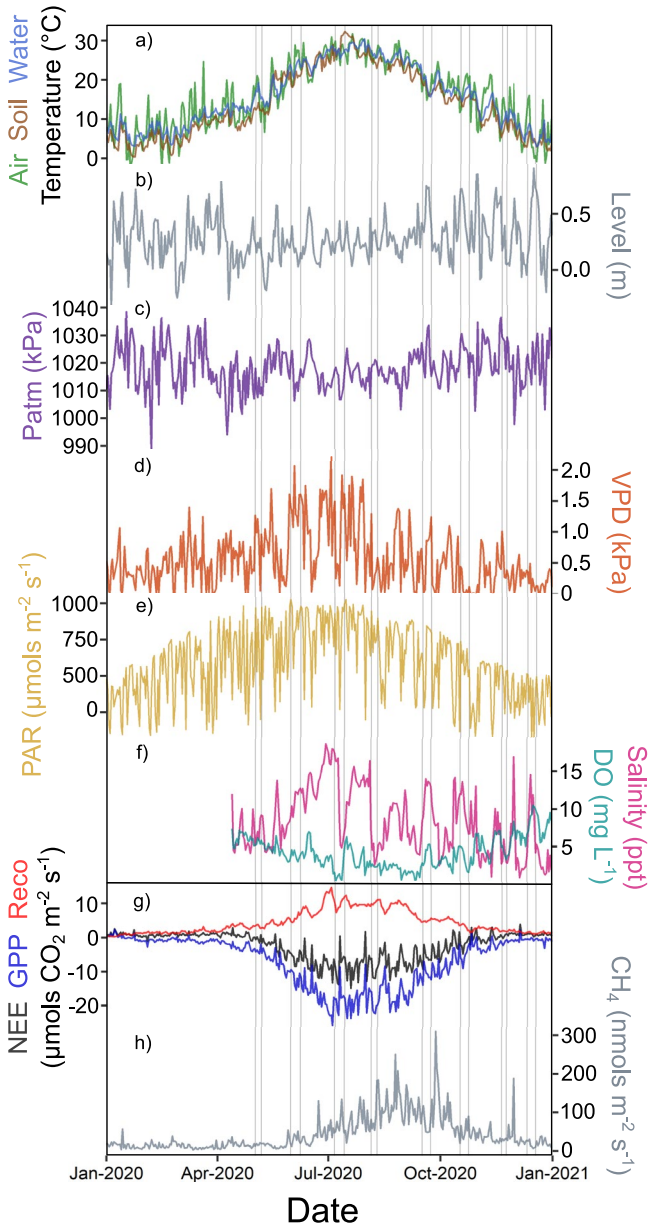

Figure 1. Daily data for (a) air (green), sediments (brown) and water temperature (blue), (b) water level (gray), (c) atmospheric pressure (purple), (d) vapor pressure deficit (VPD; orange), (e) photosynthetically active radiation (PAR; gold), (f) creek salinity (magenta) and dissolved oxygen (DO; teal), (g) ecosystem scale net ecosystem exchange (NEE; black), ecosystem scale gross primary productivity (GPP; blue), ecosystem scale respiration (Reco; red), and (h) ecosystem scale CH_4 emissions (gray). Vertical gray lines represent plot measurement days.

This mainly occurred with highly auto-correlated variables such as soil, water and air temperature. In such cases we looked at the bivariate correlation analysis and selected the driver with the best fit. The resulting variable sets were run through a dredging function which included any ecologically relevant combination of first-order interactions (MuMIn R package; Barton & Barton, 2015). All possible variable combinations were evaluated and ranked by minimal Akaike Information Criterion (AIC). Final models were chosen based on a parsimonious approach (lowest AIC with the least number of interactions).

2.6.3. Upscaling of Plot Chamber Fluxes

To examine the potential of plot measurements for upscaling applications we applied the multivariate statistical models parameterized from plot data in a predictive framework. Specifically, we left variables with similar magnitudes and ranges unscaled and applied the plot model parameters to predict fluxes using the relevant independent variables. For CH_4 and Reco emission models, where we adjusted the dependent variables, coefficients were back-transformed. Prediction uncertainty was estimated with a 95% confidence interval applied to coefficients. Daily daytime ancillary data was used in upscaling models for prediction of a daily daytime average flux rate. Likewise, the daily daytime averaged eddy covariance flux rates were used as a comparison benchmark. To arrive at annual sums from plots, we calculated the number of daytime half-hour periods each day (PAR > 20 µmols), converted predicted flux rates to half-hourly sums and multiplied by the number of daily daytime half-hour periods.

All data processing and statistical analyses were completed within R open source software version 4.0.3 (R Core Team, 2020).

3. Results

3.1. Ancillary Data and Ecosystem-Scale Carbon Exchange

Average annual temperature of the air, sediments and tidal waters were similar (14.1°C–15.6°C) as was the range of maximum temperatures (29.6°C–32.4°C), yet there was less fluctuation in sediment and water temperatures (27% narrower annual range). This was more apparent for minimum temperatures where both sediment and tidal water remained 4.5°C and 5.5°C higher than the lowest mean daily air temperature (−4.0°C), respectively. In contrast, sediment temperatures reached a daily maximum 6 days earlier than air temperature while water temperatures peaked 15 days later (29 July). Salinity and dissolved oxygen displayed opposing annual patterns with maximum daily salinity (19 ppt) and minimum dissolved oxygen (0.5 mg L^{-1}) occurring 7 days apart (5 July vs. 12 July). The wettest months were July to October which alone accounted for nearly half (350 mm, 49%) of the annual precipitation and this was immediately preceded by the driest months (May to June) (56 mm, 8%) (Figure 1).

The gap filled eddy covariance data indicated that during 2020 the ecosystem was a net source of carbon to the atmosphere with 221.7 ± 6.6 g C m^{-2} yr^{-1} from the net balance of CO_2 (NEE) and an additional 16.2 ± 0.1 g C m^{-2} yr^{-1} from CH_4. Fluxes were characteristic of highly productive tidal wetlands with CO_2 emission contributions (Reco) of 1,646 ± 1.1 g C m^{-2} yr^{-1} and GPP of 1,411.8 ± 7.1 g C m^{-2} yr^{-1}. Mean flux rates of NEE and CH_4 under daytime conditions when chambers were deployed (May to December) were −4.0 ± 4.3 µmol m^{-2} s^{-1} and 59.0 ± 48.0 nmols m^{-2} s^{-1} while mean fluxes of GPP and Reco were −9.8 ± 7.2 µmol m^{-2} s^{-1} and 5.8 ± 3.4 µmol m^{-2} s^{-1}, respectively. The 8-month period from May-December covered a majority of the active annual fluxes, capturing 100% of the annual GPP

and 87% and 88% of annual Reco and CH_4 emissions, respectively. CH_4 emissions were split evenly between day/night during this period but Reco was 52% higher under daytime conditions.

3.2. Plot-Scale Carbon Exchange

Plot chambers captured a similar seasonal pattern compared to ecosystem-scale fluxes and covered a range of environmental conditions (see Table S1 in Supporting Information S1). The overall mean NEE from semi-transparent chambers was -6.3 ± 5.0 μmol m^{-2} s^{-1} with a maximum net uptake of -13.4 μmol m^{-2} s^{-1} occurring late in maturity and maximum net emission of 0.5 μmol m^{-2} s^{-1} in dormancy. The mean GPP was -10.9 ± 8.6 μmol m^{-2} s^{-1} with a maximum and minimum uptake of -23.1 and -0.03 μmol m^{-2} s^{-1}, which occurred during the same late maturity and dormancy campaigns, respectively. Leaf-scale measurements showed an average uptake of -14.9 ± 11.4 μmol m^{-2} s^{-1} (37% higher than plot-scale GPP) with a maximum uptake of -33.5 μmol m^{-2} s^{-1} (45% higher than plot-scale GPP), that occurred during late maturity and near zero or slightly positive (net emission) (0–0.3 μmol m^{-2} s^{-1}) during dormancy. When considering the rate of uptake per unit leaf area (data not shown), the highest photosynthetic capacities were achieved early in the growing season with a progressive decline toward dormancy.

The mean Reco (dark chambers) and CH_4 emissions (semi-transparent chambers) were 4.6 ± 3.7 μmol m^{-2} s^{-1} and 18.8 ± 20.4 nmols m^{-2} s^{-1}, respectively. The highest observed Reco emissions from dark chambers was 11.2 μmol m^{-2} s^{-1}, recorded during the peak of maturity (mid-July), while average CH_4 emissions were recorded as high as 65.6 nmols m^{-2} s^{-1}, during late senescence and periodically spiked up to 294.9 nmols m^{-2} s^{-1} at the level of individual plots. Minimum Reco emissions of 0.5 μmol m^{-2} s^{-1} occurred in dormancy while minimum CH_4 emissions of 1.4–3.2 nmols m^{-2} s^{-1} were observed earlier in dormancy, just after late maturity emissions peaks. The average emission of CO_2 from sediments was 5.0 ± 4.8 μmol m^{-2} s^{-1} (8% higher than plot chamber Reco), while average emission of CH_4 from sediments was 25.8 ± 24.9 μmol m^{-2} s^{-1} (37% higher than plot chamber Reco). Despite a higher overall mean flux, peak CH_4 emission rates from sediment chambers were 71% lower than plot chamber emissions.

3.3. Representative Time Period Comparisons

Mean plot-scale NEE and GPP was similar to mean ecosystem-scale NEE and GPP from representative time periods of EC data ($p = 0.733$ and $p = 0.967$, respectively), while both Reco and CH_4 emissions were significantly higher at ecosystem-scale ($p < 0.001$ and $p = 0.01$, respectively). When examining paired time periods for each campaign day, there were significant differences between plot and ecosystem-scale NEE, GPP, Reco and CH_4 emissions in 25%, 12%, 56%, and 44% of comparisons, respectively (Figures 2a–2d). Looking at these specific cases, NEE was always greater (more negative) at plot-scale while Reco and CH_4 emissions were always greater at ecosystem-scale. Both Reco and CH_4 fluxes were associated with a period of consistent disagreement between measurement techniques which developed during late maturity and persisted through senescence and dormancy periods. Despite this, incorporating all pairwise comparisons ($n = 16$) provided good agreement with fits ranging $R^2 = 0.74$ for CH_4 fluxes to $R^2 = 0.84$ for NEE and $R^2 = 0.95$ for both GPP and Reco. Slopes for NEE, GPP and Reco were nearly 1:1 (0.99, 0.99 and 0.98, respectively), while the slope for CH_4 indicated emissions over 200% higher (slope = 3.36) for ecosystem-scale fluxes (Figures 2e–2h).

Mean leaf-scale net photosynthesis derived from leaf cuvette measurements (GPP proxy) was similar to both plot-scale ($p = 0.270$) and ecosystem-scale GPP ($p = 0.287$). Leaf-scale GPP was significantly different in 50% of the paired time periods and these cases all occurred from maturity into dormancy (Figure 3a). Incorporating all pairwise comparisons resulted in good overall agreement across techniques ($R^2 = 0.75$), yet leaf-scale GPP was over 30% higher (slope = 0.6) than ecosystem-scale fluxes (Figure 3d).

Mean Reco derived from sediment chambers was similar to plot-scale ($p = 0.926$) and ecosystem-scale Reco ($p = 0.564$). Mean CH_4 emissions from sediments were also similar to plot-scale ($p = 0.086$) and ecosystem-scale CH_4 emissions ($p = 0.196$). Although the seasonal pattern was preserved, CO_2 emissions targeted from sediments were more variable (CV = 93%) than plot-scale (CV = 84%) or ecosystem-scale Reco (CV = 75%) while CH_4 was most variable at ecosystem-scale (CV = 136%). There were significant differences between sediment and ecosystem-scale emissions of CO_2/Reco and CH_4 in 63% and 50% of the pairwise comparisons, respectively (Figures 3b and 3c). Sediment emissions were significantly lower during senescence and dormancy (63% of

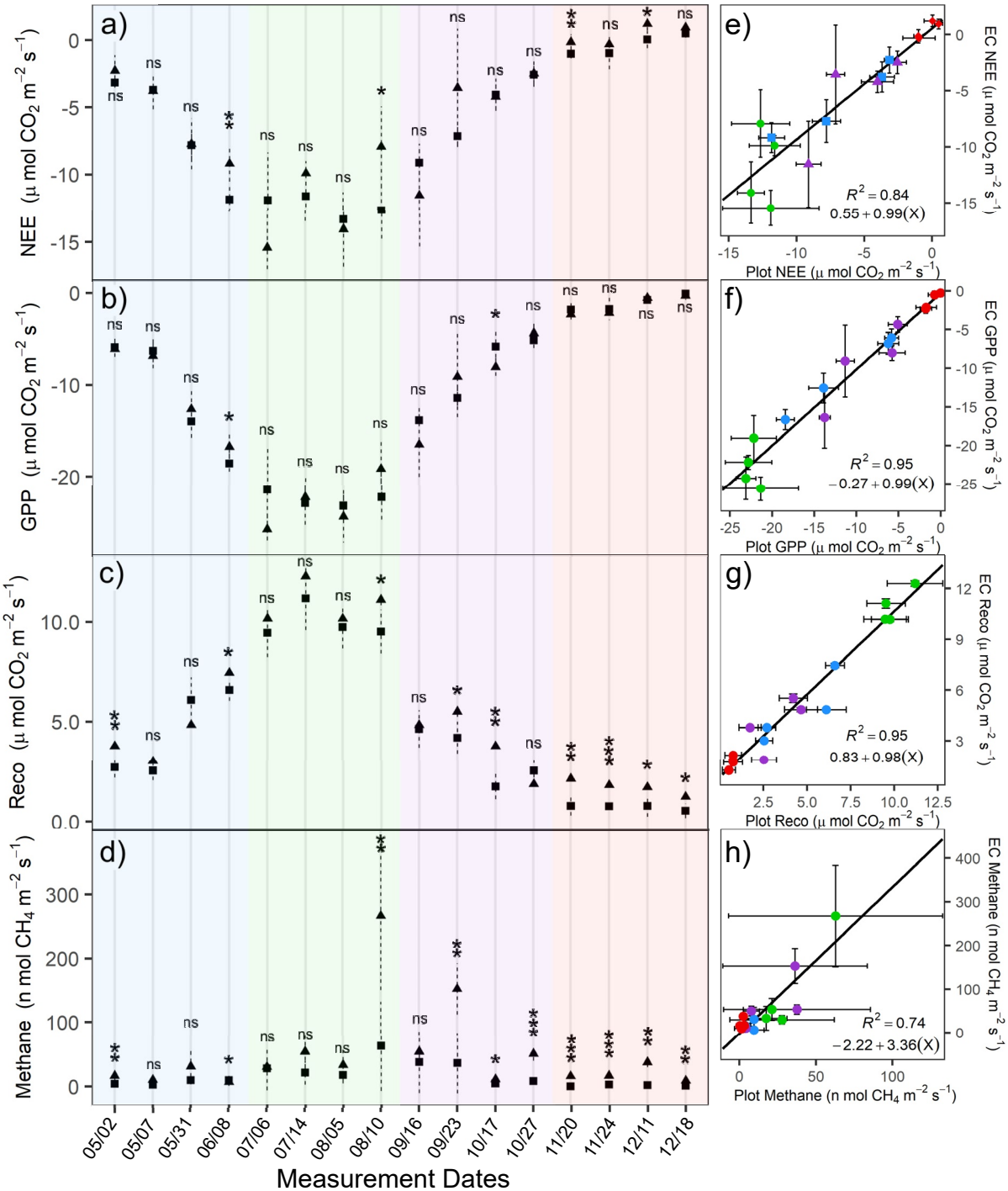

Figure 2. Comparisons between plots (black squares) and representative time periods from eddy covariance (black triangles) for: (a) net ecosystem exchange (NEE), (b) gross primary productivity (GPP), (c) respiration (Reco) and (d) CH_4 emissions; and overall regression comparisons for: (e) NEE, (f) GPP, (g) Reco and (h) CH_4 emissions. Colors represent phenology periods, blue = green-up, green = maturity, purple = senescence and red = dormancy. Error bars show ± standard deviation. Significance levels: $p < 0.001$***, $p < 0.01$**, $p < 0.05$*, ns = non-significant.

cases) but were higher during green-up (50% of cases) and had considerably lower agreement when incorporating all pairwise comparisons ($R^2 = 0.37$ for CO_2, $R^2 = 0.19$ for CH_4) with slopes indicating 50% higher (slope = 0.5) CO_2 emissions from sediments while CH_4 emissions were 33% higher (slope = 1.33) at ecosystem-scale (Figures 3e and 3f).

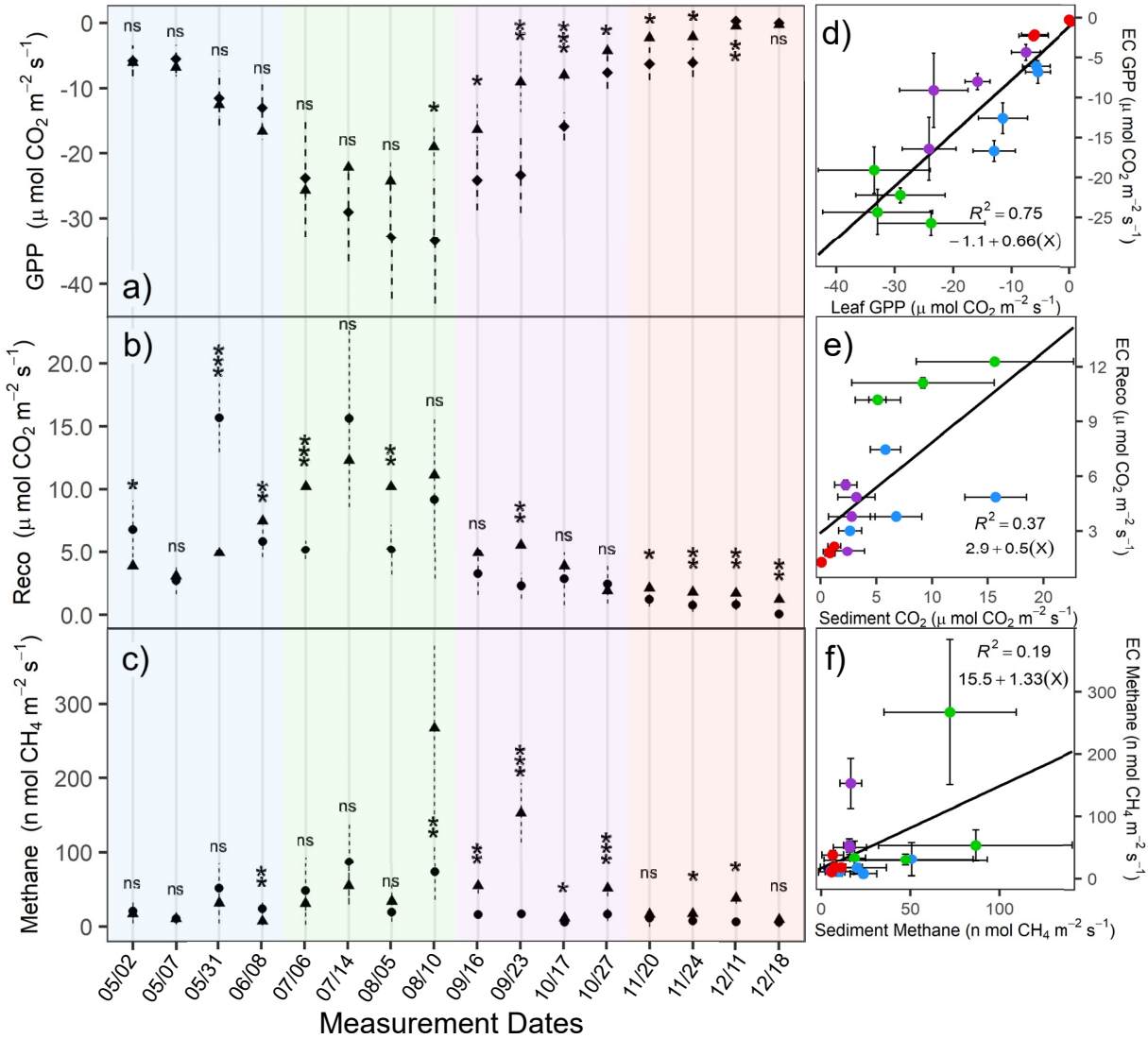

Figure 3. Comparisons between leaf-scale (black diamonds), sediment-scale (black circles) and representative time periods from eddy covariance (black triangles) for: (a) productivity/gross primary productivity (GPP), (b) sediment/ecosystem respiration (Reco) and (c) sediment/ecosystem CH_4 emissions; and overall regression comparisons for: (d) GPP, (e) Reco, (f) CH_4 emissions. Colors represent phenology periods, blue = green-up, green = maturity, purple = senescence and red = dormancy. Error bars show ± standard deviation. Significance levels: $p < 0.001$***, $p < 0.01$**, $p < 0.05$*, ns = non-significant.

3.4. Bivariate Functional Relationships

As measurements began to integrate larger spatial areas ($Plot_{exp} \rightarrow EC_{exp} \rightarrow EC_{dd}$), main drivers (e.g., temperature) provided less explanatory power while relationships strengthened for other drivers (e.g., dissolved oxygen, PAR). For NEE, relationships established at plot-scale ($Plot_{exp}$) were similar to the representative EC time periods (EC_{exp}), yet when incorporating more time-integrated data at ecosystem scale (EC_{dd}), relationships with temperature, VPD and pressure weakened while PAR and salinity strengthened. For GPP, relationships across techniques were nearly the same, although at leaf-scale there were fewer significant relationships and salinity only became significant when applying the higher level ecosystem data (EC_{dd}). There was also a positive relationship with dissolved oxygen that was consistent across techniques for both NEE and GPP ($R^2 = 0.29$–0.32).

Bi-variate relationships for Reco and CH_4 emissions followed the same patterns (i.e., variables which helped explain increased (more negative) NEE or GPP also promoted increased emissions). For Reco, the importance of temperature largely overshadowed other drivers at plot and ecosystem-scales ($R^2 = 0.92$–0.95) and while many drivers had consistent relationships across measurement techniques (i.e., VPD, DO, PAR), the negative

relationship with pressure was stronger at plot-scale and the positive relationship with salinity was only established when utilizing the higher level of ecosystem-scale data (EC_{dd}). Sediment fluxes had the least number of significant relationships and a weaker overall relationship with temperature ($R^2 = 0.73$). CH_4 emissions were complex and resulted in the fewest number of significant relationships and greater discrepancies across techniques. The temperature relationship was strongest at sediments ($R^2 = 0.70$) but weakened considerably when moving to ecosystem-scale data ($R^2 = 0.59$ for EC_{exp}, $R^2 = 0.32$ for EC_{dd}), while the negative relationship with dissolved oxygen became stronger and explained more variability than temperature ($R^2 = 0.44$) when applying more time-integrated ecosystem data (EC_{dd}) (see Figures S1–S4 in Supporting Information S1).

3.5. Statistical Modeling

Multivariate GLS models had good explanatory agreement across measurement techniques with fits ranging from $R^2 = 0.87$–0.91, 0.85–0.94, 0.92–0.99 and 0.78–0.83 for NEE, GPP, Reco and CH_4 emissions, respectively (Figure 4) (see Tables S3–S6 in Supporting Information S1). Temperature was consistently the most important driver for all components and was often the sole driver of plot fluxes. Water temperature typically had more explanatory power but when focusing on ecosystem-scale CH_4 emissions, air temperature became more relevant. Additional drivers at plot-scale included water level as a negative driver of sediment emissions and VPD as a negative driver of GPP and CH_4 emissions. When utilizing representative time periods from ecosystem-scale fluxes (EC_{exp}), water level became a weak positive driver (more negative) of both NEE and GPP, while VPD (negative effect) became as important as air temperature in explaining daily emissions of CH_4.

Applying ecosystem-scale data with more time-integration (EC_{dd}), resulted in a greater number of drivers and more complex models. The Reco model had the highest explanatory power ($R^2 = 0.99$) yet was simple with water temperature as the overwhelming driver. GPP and CH_4 were explained with an R^2 of 0.94 and 0.78, respectively, and required an increasing level of complexity. Water temperature and PAR were most important to explain GPP while opposing drivers of air temperature and dissolved oxygen were equally important to explain CH_4. Finally, NEE was explained with an R^2 of 0.87 but required the most complex model with multiple interaction terms (see Tables S1–S4 in Supporting Information S1).

3.6. Temporal Upscaling With Chamber Measurements

We used models described in Section 3.5 parameterized with data from plot chambers, leaf-cuvette measurements and sediment chambers to predict carbon fluxes along a year and compare these estimates with ecosystem-scale measurements as a benchmark (Figure 5, see Table S2 in Supporting Information S1). While predicted NEE had good overall agreement ($R^2 = 0.69$), daily average rates were significantly different across techniques ($p < 0.001$), resulting in overpredictions of 31% (slope = 0.83) compared to ecosystem-scale fluxes. Daily rates of GPP were also significantly different ($p = 0.04$) despite improved agreement ($R^2 = 0.84$) and a nearly 1:1 slope (0.99), while leaf-scale rates were higher ($p < 0.001$), resulting in overpredictions of 40% (slope = 0.60) compared to ecosystem-scale GPP. Likewise, rates of predicted CO_2 emission from sediments and Reco from plot chambers were significantly different from ecosystem-scale rates ($p = 0.010$), with sediments emissions 15% higher (slope = 0.85) while the slope for plot chamber estimates was 1:1 (1.0). Predicted CH_4 fluxes provided the weakest fits ($R^2 = 0.33$–0.35) and both sediments ($p < 0.001$) and plot chambers ($p < 0.001$) were 33% (slope = 1.33) and 76% (slope = 1.76) lower than ecosystem-scale fluxes.

Discrepancies in daily modeled rates of NEE and GPP were greatest during green-up and senescence transitional periods (over predictions) while discrepancies for Reco and CH_4 emissions were observed during dormancy (under predictions) and peak CH_4 emissions during late maturity and senescence were not captured. Estimated annual sums from plot chambers resulted in a 108% overestimation for NEE (−1055.0 vs. −521.0 g C yr^{-1}), 12% overestimation for GPP (−1,431.0 vs. −1,622.0 g C yr^{-1}), but 14% underestimation for Reco (777.0 vs. 902.0 g C yr^{-1}) and 67% underestimation for CH_4 emissions (2.7 vs. 8.3 g CH_4 C yr^{-1}) when compared with benchmark EC measurements (EC_{dd}).

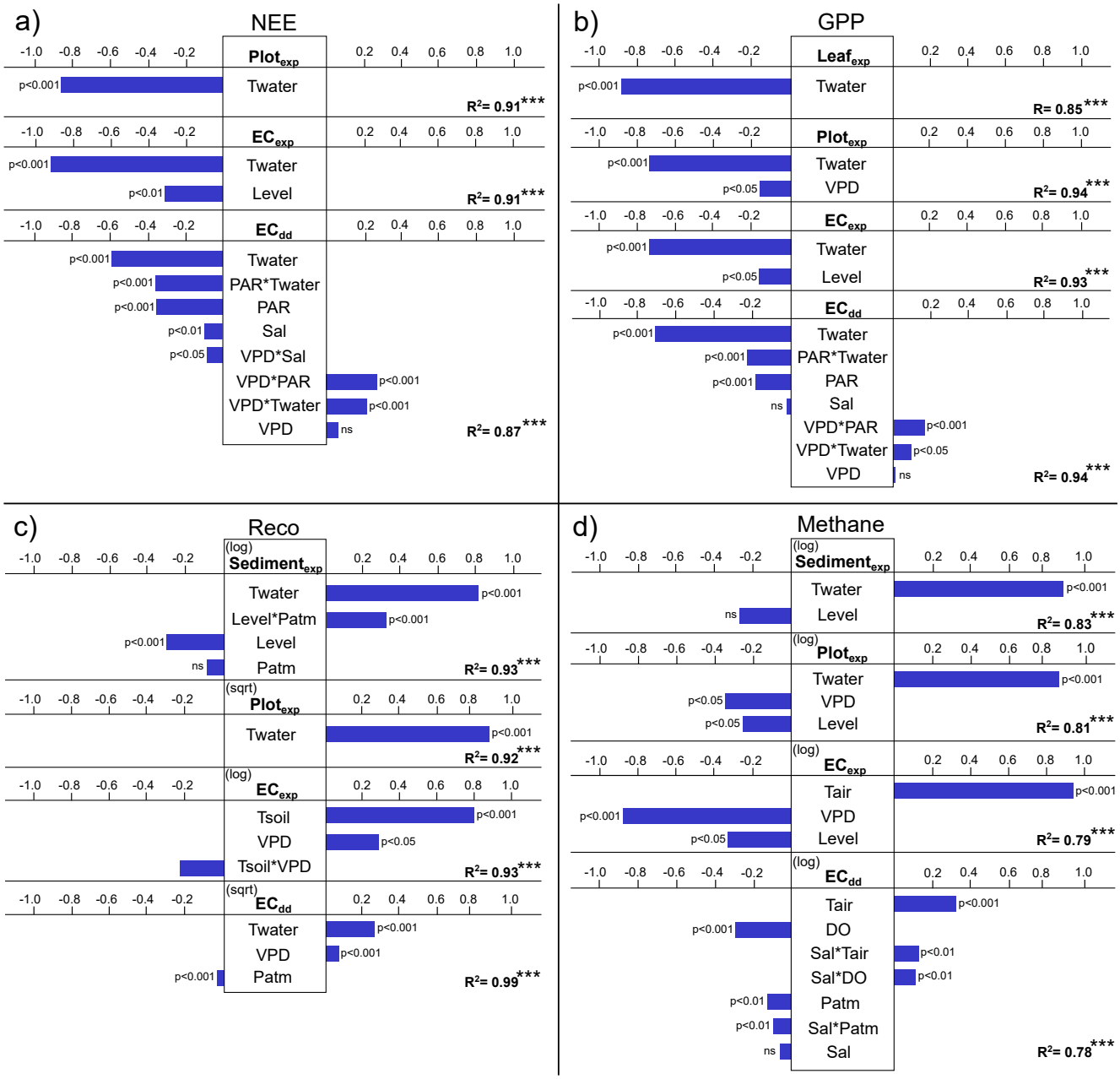

Figure 4. Generalized least squares modeling results comparing standardized coefficients for (a) net ecosystem exchange (NEE), (b) gross primary productivity (GPP), (c) respiration (Reco) and (d) CH_4 emissions; $Plot_{exp}$ = plot chamber measurements, $Leaf_{exp}$ = leaf-scale measurements, $Sediment_{exp}$ = sediment chamber measurements, EC_{exp} = representative time periods from eddy covariance and EC_{dd} = daily daytime eddy covariance data. Note: p-values denote level of coefficient significance in a multivariate context. Significance levels: $p < 0.001$***, $p < 0.01$**, $p < 0.05$*, ns = non-significant.

4. Discussion

We examine CH_4 and CO_2 fluxes using a combination of chamber and eddy covariance measurements in a temperate salt marsh. Our first hypothesis (H1), was generally supported, yet the level of agreement between plot and ecosystem-scale measurements was dependent on phenology, especially regarding carbon emissions (i.e., Reco and CH_4). Leaf-scale measurements showed a steady decline in photosynthetic efficiency over time but when accounting for plot leaf area, rates exceeded EC-derived GPP well into dormancy phenophase. Emissions of CH_4 and CO_2 directly from sediments were more variable compared to plot chambers, yet agreement between measurement techniques was also linked to canopy phenological stages. Our second set of hypotheses (H2,

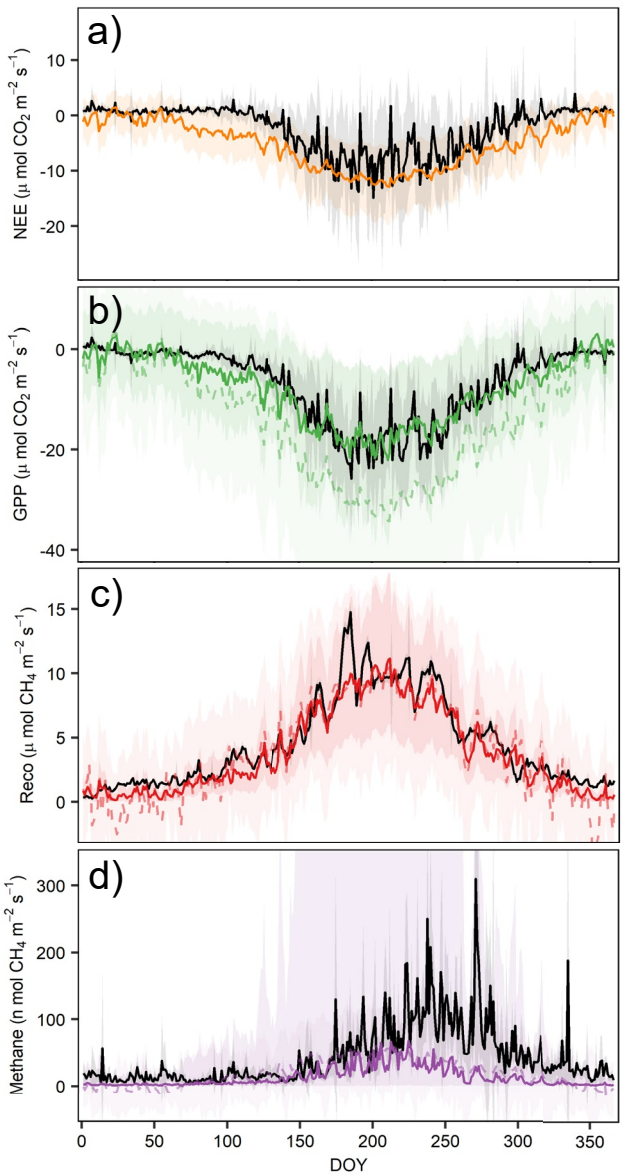

Figure 5. Daily daytime rates of (a) net ecosystem exchange (NEE), (b) gross primary productivity (GPP), (c) respiration (Reco) and (d) CH_4 emission estimated with modeling parameters from plot chambers (solid colored lines), leaf/sediment chambers (colored dashed lines) and daily daytime eddy covariance data as a benchmark (solid black lines).

H3), regarding functional relationships, environmental drivers and temporal upscaling between measurement techniques was only partially supported. We found that functional relationships were mostly preserved across techniques but in many cases when applying data with more temporal integration (EC_{dd}), complexities of the larger system were revealed. Likewise, multivariate models became more complex with numerous interaction terms for measurement techniques which integrate larger spatial variability.

4.1. Ecosystem-Scale Carbon Exchange

The annual NEE was 221.7 ± 6.6 g C m^{-2} yr^{-1} with an additional 16.2 ± 0.1 g C m^{-2} yr^{-1} from CH_4 which is 60% higher net carbon loss than net fluxes recorded between 2015 and 2017 (Vazquez-Lule & Vargas, 2021) suggesting large interannual variability in carbon dynamics of salt marshes. Many studies have reported that tidal wetlands act as net carbon sinks as low as −901 g C m^{-2} yr^{-1} from a native Phragmites marsh (Huang et al., 2020) or net carbon sources as high as 984 g C m^{-2} yr^{-1} from a restored urban marsh (Schafer et al., 2014). Despite a comparable net carbon balance with other temperate tidal wetlands, magnitudes of GPP and Reco were 72% and 179% higher than those from a northern temperate marsh (Forbrich et al., 2018), and 44% and 114% higher than those from another mid-Atlantic marsh, respectively (Artigas et al., 2015). Our annual budgets of GPP and Reco are comparable with those reported from tropical mangrove systems or highly productive Eastern marshes (Ge et al., 2015; Lu et al., 2017). Our annual methane budget (16.2 ± 0.1 g C m^{-2} yr^{-1}) also falls on the high end of reported emissions from other salt marshes sites (11–13.8 g C m^{-2} yr^{-1}) (Holm et al., 2016; Krauss et al., 2016) yet was similar to Li et al. (2018) (17.6 g C m^{-2} yr^{-1}) where both the salinity range (0–25 ppt) and species dominance (*S. alterniflora*) coincide with our site.

4.2. Plot-Scale Fluxes

Studies applying plot-scale measurements within tidal wetlands are scarce due to challenges of the environment including tidal cycles. We propose that it is critical to consider a broad suite of environmental conditions when applying chamber-based measurements to estimate carbon budgets or for accounting applications as tides can have a strong influence on gas exchange (Huang et al., 2020; Wei et al., 2020). Several studies have found a variable response of NEE to tides highlighting the importance of site-specific conditions (Guo et al., 2009; Knox et al., 2018; Nahrawi et al., 2020). We found that NEE was 19.3% lower (more negative) when considering only high tide days which could be attributed to a suppression of Reco via the water barrier that limits oxygen diffusion to sediments, promoting less metabolically favorable conditions (Seyfferth et al., 2020), while directly impeding atmospheric emissions (Emery et al., 2021; Huang et al., 2020). Toxic metabolites could also be more readily flushed from the rhizosphere or terminal electron acceptors replenished (sulfide → sulfate), possibly reducing vegetation stress (Forbrich & Giblin, 2015; Guo et al., 2009; Pezeshki, 2001).

The overall mean plot-scale Reco (4.6 μmol m^{-2} s^{-1}) fell within the range (4.2–5.8 μmol m^{-2} s^{-1}) reported by two previous canopy chamber studies from *S. alterniflora* marshes (Xu et al., 2014; Yang et al., 2018). That said, our measurements were considerably higher than those at another US East Coast site (approximately 523 km away), where Reco was nearly balanced with GPP for plots located within the marsh interior (net exchange of 5.0 g C m^{-2} yr^{-1}) (Czapla et al., 2020b). These differences are likely driven by tidal range relative to platform height as our site has a greater mean elevation (0.6 m vs. −0.04 m) and range (1.7 vs. 0.83 m) than Czapla et al. (2020b) leading to more dynamic water table fluctuations and a diverse range of biogeochemical conditions (Seyfferth

et al., 2020). Chamber measurements of CH_4 which incorporate the plant canopy are generally more variable than CO_2 within tidal wetlands with single maximum emissions reported as high as 1,250 nmols m^{-2} s^{-1} (325% higher than our peak rates) and as low as 4.3 nmols m^{-2} s^{-1} (over 6,000% lower) (Czapla et al., 2020b; Yang et al., 2021). Our mean rate was still 334%–487% higher than several *S. alterniflora* marshes and emissions were considerably more seasonal with maximum rates developing during late maturity and senescence (Czapla et al., 2020b; Geoghegan et al., 2018; Xu et al., 2014), potentially indicating that freshly degraded plant compounds are providing an electron source for non-competitive methylotrophic methanogenesis (Seyfferth et al., 2020).

4.3. Plot to Ecosystem-Scale Comparisons

At plot-scale, components related to plant activity (NEE and GPP) had the best overall agreement with ecosystem-scale fluxes ($R^2 = 0.84$–0.95) and the fewest number of differences among pairwise comparisons. Over 66% of the integrated EC footprint is associated with short form *S. alterniflora* (Vazquez-Lule & Vargas, 2021), which helps constrain possible explanations for discrepancies across measurement techniques. NEE and GPP are also reliant on physiological properties of vegetation and are associated with slower environmental response (e.g., stomatal conductance and photosynthetic capacity) which helps constrain any abrupt variability of fluxes and there is less influence from physical forcings such as pressure and water level (Villa et al., 2021), which could further contribute to the higher level of agreement with these components.

Plot-scale carbon emissions (i.e., Reco and CH_4 fluxes) also had good agreement with ecosystem fluxes ($R^2 = 0.74$–0.95), yet the level of agreement between pairwise comparisons was dependent on phenology. We postulate a combination of physical and biogeochemical differences across the marsh where chambers are located and the broader ecosystem as possible explanations driving these discrepancies. First, EC measurements integrate tidal channels and flanking vegetation associated with higher biomass, larger culms and deeper rooting depth which likely leads to greater CO_2 respiratory costs from increased canopy shading late in the growing season (Dingkuhn et al., 1990). This also likely drives heterogeneous methane production and emissions via increased photoassimilate transport and plant mediated pathways (Seyfferth et al., 2020). Second, tidal waters remain warmer than sediment and air temperatures later into dormancy which could cause increased heterogeneity in sediment respiration rates. Third, since higher biomass correlates with increased sediment deposition in tidal systems (Kirwan & Megonigal, 2013; Kirwan et al., 2016), and sediments in this zone are found to have courser textures (Seyfferth et al., 2020), it is likely that tidal cycling increases the potential for allochthonous carbon and nutrient deposition, providing additional substrates for the microbiome (Czapla et al., 2020a). Lastly, the range and depth of tidal flow may not be consistent across seasons. When looking at monthly average water levels during the study, we find that under daytime conditions when chambers were deployed, water levels were 70% higher from September-December (0.34 m) than from May to August (0.20 m) which could have suppressed emissions from interior region relative to higher elevation levees where sediments remain more oxygenated (Kostka et al., 2002).

We found that maximum emissions from chambers were 80% and 24% lower than CH_4 and CO_2 fluxes measured by EC. This was in opposition to findings of Krauss et al. (2016) where respiratory CH_4 and CO_2 emissions were compared over 5 sampling periods at a brackish Gulf Coast marsh populated by *S. patens*. Although pairwise comparisons with representative time periods from EC were not explicitly tested, maximum emissions recorded from chambers were 317% and 44% higher than CH_4 and CO_2 fluxes measured by EC, respectively. One contrasting feature is the limited microtidal range and sediment supply of Gulf Coast marshes (Holmquist et al., 2021). This acts to restrict deposition and levee development resulting primarily in vegetated flats or areas of open water which persistently occupies a higher proportion of the total area. Thus, while the plot-scale fluxes were likely representative of contributions from vegetated flats, considerable areas of open water and tidal creeks were also integrated with EC where fluxes are likely lower or masked by lateral transport across system boundaries (Cai, 2011; Trifunovic et al., 2020).

4.4. Bivariate Functional Relationships

Strong functional relationships for NEE and GPP were established with each measurement technique but with greater spatiotemporal integration (EC_{dd}), the effect of temperature weakened while the importance of other drivers increased. This highlights the dynamic nature of tidal wetlands as tidal cycles can cause a dynamic

co-variation and confounding effects among water level, salinity and dissolved oxygen (Abdul-Aziz et al., 2018; Moffett & Gorelick, 2016; Vazquez-Lule & Vargas, 2021), which can manifest at a variety of temporal scales (Knox et al., 2018). In many cases, plot-scale measurements only provide a snapshot within the diurnal cycle, which in our case still provided strong bi-variate relationships with variables having stronger seasonal linkages (i.e., temperature) but failed to capture the importance of variables having a stronger diurnal linkage (i.e., PAR).

Relationships established for Reco were also similar across scales, but the overwhelming effect of temperature was preserved even with a higher level of data coverage. While temperature is important, Reco values derived from our EC measurements are generated from a model using temperature (nighttime method) (Reichstein et al., 2005). That said, there is direct evidence that temperature is a very strong driver of sediment respiration at this site (Capooci & Vargas, 2022). We recognize that nighttime Reco is not the same as nighttime sediment respiration (Barba et al., 2019), but also incorporates vegetation which supports the larger disconnections found between sediment emissions derived from sediment chambers ($R^2 = 0.73$) and plot-scale Reco derived from plot chambers ($R^2 = 0.88$).

Our results show that functional relationships for CH_4 fluxes are complex. While temperature is important, its effect is bi-directional, promoting both increased production and oxidation (Morin et al., 2014; Rey-Sanchez et al., 2018), which can confound the overall response when analyzed throughout a year. When applying daily daytime data, we found the negative influence of dissolved oxygen explained more variability than any other driver ($R^2 = 0.44$). Since dissolved oxygen oscillates seasonally with highest levels during dormancy when CH_4 fluxes are lowest, this could be causing another spurious correlation, albeit a biologically expected relationship as higher dissolved oxygen promotes CH_4 oxidation and reduces atmospheric CH_4 emissions (Trifunovic et al., 2020). Supporting this are findings from a freshwater study where temperature was a less important regulator of oxidation compared to dissolved oxygen (Thottathil et al., 2019). Despite the importance of salinity as a negative control on CH_4 emissions reported by many studies (Al-Haj & Fulweiler, 2020; Krauss et al., 2016; Tong et al., 2010), we found no significant relationship using data from chambers or EC despite levels up to 18.5 ppt and half-hourly levels up to 23.4 ppt. These salinity values place our site on the upper echelon of the widely accepted salinity/CH_4 limitation threshold (Poffenbarger et al., 2011), but it has been proposed that CH_4 production in our site is driven by noncompetitive methylotrophic methanogenesis (Seyfferth et al., 2020) which challenges the current paradigm of CH_4 production limitation driven by salinity gradients.

4.5. Statistical Modeling Across Measurement Techniques

The use of bivariate relationships provides a standardized way to examine how the response of individual variables changes across measurement techniques. However, within a complex system important variable dependencies and interactions can arise, thus multivariate models can help reveal additional information about each measurement technique and the associated data. Temperature was still the overwhelming factor regardless of measurement techniques but additional drivers were identified. For plot-scale data, VPD was a negative driver of plot CH_4 emission yet promoted carbon uptake (GPP). This effect is likely linked to stomatal conductance and dissolved methane in the transpiration stream (Megonigal & Guenther, 2008; Mitra et al., 2020), while CO_2 uptake rates are somewhat promoted due to high concentrations of CO_2 in bundle-sheath cells of *Spartina* vegetation (C4 pathway) which could temporarily increase water use efficiency when conductance becomes limited (Ye et al., 2020). Water level was a negative driver of both sediment Reco and CH_4, indicating physically slowed rates of sediment-atmosphere diffusion when sediments become saturated (Emery et al., 2021; Li et al., 2018).

When applying representative time periods from EC which aligned with the timing of plot measurements, higher water levels promoted carbon uptake (more negative NEE and GPP) and suppressed CH_4 emissions which is in-line with a previous site study (Vazquez-Lule & Vargas, 2021). Adding to the previous findings, we attribute this response to several factors including tidal range, site geomorphology, sediment biogeochemistry and platform elevation which at our site, limits any significant inundation of vegetation that would temporarily reduce photosynthetic leaf area yet sediments still become regularly flooded (Hill, Vázquez-Lule, & Vargas, 2021). This can provide a flushing effect to interior sediments where sulfides limit plant growth (Lamers et al., 2013), while temporarily suppressing emissions (Emery et al., 2021). Likewise, persistently saturated conditions and low Eh values in interior sediments promotes a methanogenic environment resulting in large subsurface CH_4 pools (Seyfferth et al., 2020), where emissions become highly regulated by hydrological controls. In fact, many wetland studies finding opposing patterns, were dominated by *P. australis* stands which can greatly increase plant

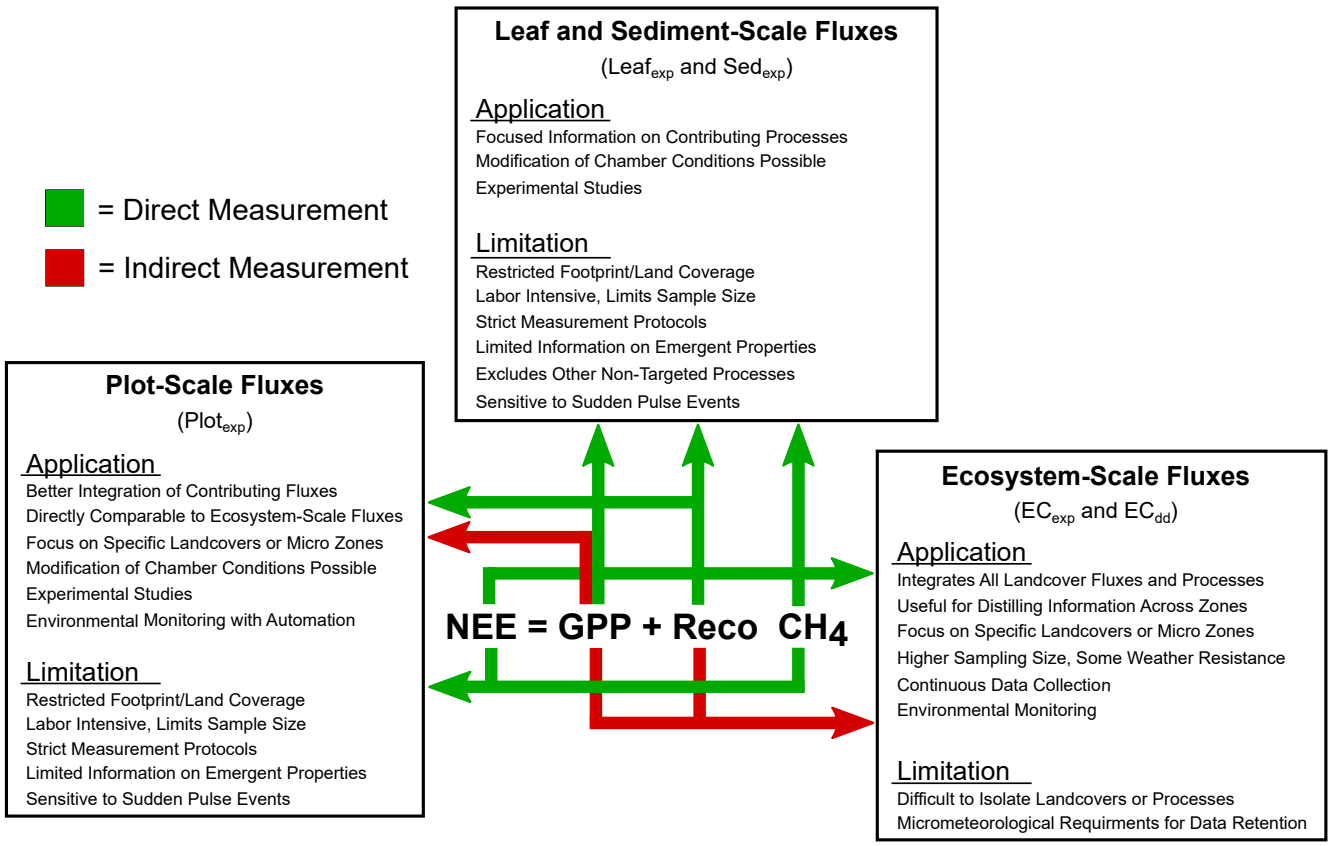

Figure 6. Primary application and limitation of different scales of measurement and levels of data coverage. Green arrows represent direct measurements, red arrows represent indirect or inferred measurements. $Leaf_{exp}$ = leaf-scale measurements, Sed_{exp} = sediment chamber measurements, $Plot_{exp}$ = plot chamber measurements, EC_{exp} = representative time periods from eddy covariance and EC_{dd} = daily daytime averaged eddy covariance data.

mediated emissions, thus by-passing any water barriers (Liu et al., 2019; Olsson et al., 2015), or only experienced seasonal flooding (Knox et al., 2021). Further supporting this line of evidence are findings from Huang et al. (2019) that air exposed sediments had greater emissions during high tide season compared to low tide season when sediments are less frequently flooded.

When applying the higher level of EC data which integrates all daytime measurements (EC_{dd}), there were numerous interaction terms and sub-daily water level oscillations were no longer significant for any flux component. Despite this, tidally regulated salinity and dissolved oxygen were significant interactive variables for NEE and CH_4, likely exerting influence on terminal electron replenishment and methane oxidation rates (Pezeshki, 2001; Tobias & Neubauer, 2019). Further, VPD and PAR were significant interactive variables regulating NEE and GPP, likely exerting influence on stomatal conductance and rates of photosynthesis (Kathilankal et al., 2011). Consistent with bivariate functional relationships, the regulation of CH_4 flux by dissolved oxygen remained equally important as temperature.

4.6. Implications and Considerations to Reconcile Measurement Approaches

Each measurement technique which we included has a set of best use applications but also limitations (Figure 6). This is primarily tied to the amount of spatial and temporal data integration but also technical factors, ease of implementation and cost. Plot chamber derived fluxes which incorporate both sediments and the full plant canopy can provide an accurate snapshot of ecosystem fluxes, offer direct measurements of GPP and Reco and targeted fluxes from sediments and vegetation can provide detailed information about contributing processes. While chambers could be more feasible for manipulation studies, chamber surveys can typically identify the strongest/most relevant drivers and improved monitoring for detailed system characterization or budgets could also be possible with automation (Hill, Barba, et al., 2021). Despite these applications, chamber based methods have a restrictive

sampling footprint, are labor intensive with strict sampling protocols, can be sensitive to pulses or hotspots and may fail to capture emergent properties of the larger system. Eddy covariance derived fluxes are more fully integrated across the whole ecosystem and while there are still challenges for data inclusion during periods of low turbulence or storm events, collection is possible over longer intervals which provides better information for characterization or annual budgets. Often the limitation of one method is complemented by the strength of another. While the use of a specific method is largely dependent upon research goals and available resources, combining multiple techniques can provide a powerful way to understand multi-level system dynamics.

Within tidal wetlands, when applying chamber methods for ecosystem-scale metrics, we advocate for larger chambers when possible which are able integrate a larger footprint that helps reduce flux variability or pulse effects. This approach can be paired with targeted measurements of sediment and vegetation to fully understand the contributing fluxes integrated within the chamber. When running an eddy covariance system, we advocate for periodic chamber field surveys for sanity checks, constraining the magnitude of partitioned fluxes (GPP, Reco) and for assessing contributions to ecosystem level fluxes.

5. Conclusions

We systematically compared measurement techniques which integrate information across different spatial and temporal scales within a temperate salt marsh. This approach was helpful to understand the potential applications and limitations of each technique while combining techniques allowed for more information on system functionality. When placing chambers within the representative EC footprint, we found good overall agreement between paired plot chambers and EC. We generally saw that agreement was more consistent for NEE and GPP and decreased for CH_4 and Reco emission components during senescence and dormancy, supporting the idea of more biological activity associated with tidal creeks/levees that only EC was able to integrate at ecosystem-scale. We found it was important to include a variety of conditions including variable water levels for chamber measurements, as the magnitude of emission fluxes was reduced with elevated water levels. Bivariate functional relationships provided evidence that the influence of drivers was dependent on the scale of the measurement and multivariate statistical modeling revealed that while the system was characterized well at plot-scale (mainly via temperature), including a more comprehensive data set (EC_{exp} and EC_{dd}) revealed higher system complexities. Applying empirical upscaling models from plot measurements resulted in overpredictions of NEE and GPP and underpredictions of CH_4 and Reco emissions which indicates that periodic chamber measurements underestimate the complexity of a dynamic system. Our findings ultimately support the need for continuous monitoring within these ecosystems as limited data coverage can lead to omissions of important secondary drivers and variable interactions which can generate greater uncertainty or errors when solely utilizing chamber based data.

Data Availability Statement

Meteorological (station: delsjmet-p) and water quality (station: Aspen Landing) data are available from the National Estuarine Research Reserve's Centralized Data Management Office (CDMO) at https://cdmo.baruch.sc.edu/. Phenological data are available from the PhenoCam network (site: stjones) at https://phenocam.sr.unh.edu/webcam/sites/stjones/. Eddy covariance data are available via AmeriFlux (US-StJ; https://ameriflux.lbl.gov/sites/siteinfo/US-StJ). Chamber data, along with ancillary measurements of leaf-level photosynthesis and LAI are available on Figshare at the following https://doi.org/10.6084/m9.figshare.20099321.

Acknowledgments
This research was supported by the National Science Foundation (#1652594) and the Department of Energy (DE-SC0022185). AH acknowledges support from the Delaware Environmental Institute, the National Science Foundation EPSCoR (#1757353) and the State of Delaware. We thank the onsite support from the Delaware National Estuarine Research Reserve (DNERR), as well as from Jack Hill for field assistance during all campaigns. We thank Inke Forbrich and Karina Schafer for inspiring discussions about carbon fluxes in salt marshes. The authors acknowledge the land on which they conducted this study is the traditional home of the Lenni-Lenape tribal nation (Delaware nation).

References

Abdul-Aziz, O. I., Ishtiaq, K. S., Tang, J. W., Moseman-Valtierra, S., Kroeger, K. D., Gonneea, M. E., et al. (2018). Environmental controls, emergent scaling, and predictions of greenhouse gas (GHG) fluxes in coastal salt marshes. *Journal of Geophysical Research: Biogeosciences*, *123*(7), 2234–2256. https://doi.org/10.1029/2018jg004556

Acosta, M., Dusek, J., Charnizo, S., Serrano-Ortiz, P., & Pavelka, M. (2019). Autumnal fluxes of CH_4 and CO_2 from Mediterranean reed wetland based on eddy covariance and chamber methods. *Catena*, *183*, 104191. https://doi.org/10.1016/j.catena.2019.104191

Al-Haj, A. N., & Fulweiler, R. W. (2020). A synthesis of methane emissions from shallow vegetated coastal ecosystems. *Global Change Biology*, *26*(5), 2988–3005. https://doi.org/10.1111/gcb.15046

Alongi, D. M. (2020). Carbon balance in salt marsh and mangrove ecosystems: A global synthesis. *Journal of Marine Science and Engineering*, *8*(10), 767. https://doi.org/10.3390/jmse8100767

Artigas, F., Shin, J. Y., Hobble, C., Marti-Donati, A., Schafer, K. V. R., & Pechmann, I. (2015). Long term carbon storage potential and CO_2 sink strength of a restored salt marsh in New Jersey. *Agricultural and Forest Meteorology*, *200*, 313–321. https://doi.org/10.1016/j.agrformet.2014.09.012

Aubinet, M., Vesala, T., & Papale, D. (2012). *Eddy covariance: A practical guide to measurement and data analysis*. Springer Science & Business Media. https://doi.org/10.1007/978-94-007-2351-1

Baldocchi, D. D. (2003). Assessing the eddy covariance technique for evaluating carbon dioxide exchange rates of ecosystems: Past, present and future. *Global Change Biology*, *9*(4), 479–492. https://doi.org/10.1046/j.1365-2486.2003.00629.x

Barba, J., Cueva, A., Bahn, M., Barron-Gafford, G. A., Bond-Lamberty, B., Hanson, P. J., et al. (2018). Comparing ecosystem and soil respiration: Review and key challenges of tower-based and soil measurements. *Agricultural and Forest Meteorology*, *249*, 434–443. https://doi.org/10.1016/j.agrformet.2017.10.028

Barba, J., Poyatos, R., Capooci, M., & Vargas, R. (2021). Spatiotemporal variability and origin of CO_2 and CH_4 tree stem fluxes in an upland forest. *Global Change Biology*, *27*(19), 4879–4893. https://doi.org/10.1111/gcb.15783

Barba, J., Poyatos, R., & Vargas, R. (2019). Automated measurements of greenhouse gases fluxes from tree stems and soils: Magnitudes, patterns and drivers. *Scientific Reports*, *9*(1), 4005. https://doi.org/10.1038/s41598-019-39663-8

Barton, K., & Barton, M. K. (2015). Package 'mumin'. *Version*, *1*(18), 439.

Cai, W.-J. (2011). Estuarine and coastal ocean carbon paradox: CO_2 sinks or sites of terrestrial carbon incineration? *Annual Review of Marine Science*, *3*(1), 123–145. https://doi.org/10.1146/annurev-marine-120709-142723

Capooci, M., Barba, J., Seyfferth, A. L., & Vargas, R. (2019). Experimental influence of storm-surge salinity on soil greenhouse gas emissions from a tidal salt marsh. *Science of the Total Environment*, *686*, 1164–1172. https://doi.org/10.1016/j.scitotenv.2019.06.032

Capooci, M., & Vargas, R. (2022). Diel and seasonal patterns of soil CO_2 efflux in a temperate tidal marsh. *Science of the Total Environment*, *802*, 149715. https://doi.org/10.1016/j.scitotenv.2021.149715

Chaichana, N., Bellingrath-Kimura, S. D., Komiya, S., Fujii, Y., Noborio, K., Dietrich, O., & Pakoktom, T. (2018). Comparison of closed chamber and eddy covariance methods to improve the understanding of methane fluxes from rice paddy fields in Japan. *Atmosphere*, *9*(9), 356. https://doi.org/10.3390/atmos9090356

Cueva, A., Bullock, S. H., Lopez-Reyes, E., & Vargas, R. (2017). Potential bias of daily soil CO_2 efflux estimates due to sampling time. *Scientific Reports*, *7*(1), 11925. https://doi.org/10.1038/s41598-017-11849-y

Czapla, K. M., Anderson, I. C., & Currin, C. A. (2020b). Net ecosystem carbon balance in a North Carolina, USA, salt marsh. *Journal of Geophysical Research: Biogeosciences*, *125*(10). https://doi.org/10.1029/2019jg005509

Czapla, K. M., Anderson, I. C., & Currin, C. A. (2020a). The effect of fertilization on biomass and metabolism in North Carolina salt marshes: Modulated by location-specific factors. *Journal of Geophysical Research: Biogeosciences*, *125*(10). https://doi.org/10.1029/2019jg005238

Dingkuhn, M., Schnier, H. F., De Datta, S. K., Dörffling, K., Javellana, C., & Pamplona, R. (1990). Nitrogen fertilization of direct-seeded flooded vs. transplanted rice: II. interactions among canopy properties. *Crop Science*, *30*(6), 1284–1292. https://doi.org/10.2135/cropsci1990.0011183X003000060025x

Emery, H. E., Angell, J. H., Tawade, A., & Fulweiler, R. W. (2021). Tidal rewetting in salt marshes triggers pulses of nitrous oxide emissions but slows carbon dioxide emission. *Soil Biology and Biochemistry*, *156*, 108197. https://doi.org/10.1016/j.soilbio.2021.108197

Feagin, R., Forbrich, I., Huff, T., Barr, J., Ruiz-Plancarte, J., Fuentes, J., et al. (2020). Tidal wetland gross primary production across the continental United States, 2000–2019. *Global Biogeochemical Cycles*, *34*(2), e2019GB006349. https://doi.org/10.1029/2019GB006349

Forbrich, I., & Giblin, A. E. (2015). Marsh-atmosphere CO_2 exchange in a New England salt marsh. *Journal of Geophysical Research: Biogeosciences*, *120*(9), 1825–1838. https://doi.org/10.1002/2015jg003044

Forbrich, I., Giblin, A. E., & Hopkinson, C. S. (2018). Constraining marsh carbon budgets using long-term C Burial and contemporary atmospheric CO_2 fluxes. *Journal of Geophysical Research: Biogeosciences*, *123*(3), 867–878. https://doi.org/10.1002/2017jg004336

Forbrich, I., Kutzbach, L., Wille, C., Becker, T., Wu, J. B., & Wilmking, M. (2011). Cross-evaluation of measurements of peatland methane emissions on microform and ecosystem scales using high-resolution landcover classification and source weight modelling. *Agricultural and Forest Meteorology*, *151*(7), 864–874. https://doi.org/10.1016/j.agrformet.2011.02.006

Fox, A. M., Huntley, B., Lloyd, C. R., Williams, M., & Baxter, R. (2008). Net ecosystem exchange over heterogeneous Arctic tundra: Scaling between chamber and eddy covariance measurements. *Global Biogeochemical Cycles*, *22*(2). https://doi.org/10.1029/2007gb003027

Ge, Z. M., Guo, H. Q., Zhao, B., & Zhang, L. Q. (2015). Plant invasion impacts on the gross and net primary production of the salt marsh on eastern coast of China: Insights from leaf to ecosystem. *Journal of Geophysical Research-Biogeosciences*, *120*(1), 169–186. https://doi.org/10.1002/2014jg002736

Geoghegan, E. K., Caplan, J. S., Leech, F. N., Weber, P. E., Bauer, C. E., & Mozdzer, T. J. (2018). Nitrogen enrichment alters carbon fluxes in a New England salt marsh. *Ecosystem Health and Sustainability*, *4*(11), 277–287. https://doi.org/10.1080/20964129.2018.1532772

Guo, H. Q., Noormets, A., Zhao, B., Chen, J. Q., Sun, G., Gu, Y. J., et al. (2009). Tidal effects on net ecosystem exchange of carbon in an estuarine wetland. *Agricultural and Forest Meteorology*, *149*(11), 1820–1828. https://doi.org/10.1016/j.agrformet.2009.06.010

Heikkinen, J. E. P., Maljanen, M., Aurela, M., Hargreaves, K. J., & Martikainen, P. J. (2002). Carbon dioxide and methane dynamics in a sub-Arctic peatland in northern Finland. *Polar Research*, *21*(1), 49–62. https://doi.org/10.1111/j.1751-8369.2002.tb00066.x

Hendriks, D. M. D., van Huissteden, J., & Dolman, A. J. (2010). Multi-technique assessment of spatial and temporal variability of methane fluxes in a peat meadow. *Agricultural and Forest Meteorology*, *150*(6), 757–774. https://doi.org/10.1016/j.agrformet.2009.06.017

Hill, A. C., Barba, J., Hom, J., & Vargas, R. (2021). Patterns and drivers of multi-annual CO_2 emissions within a temperate suburban neighborhood. *Biogeochemistry*, *152*(1), 35–50. https://doi.org/10.1007/s10533-020-00731-1

Hill, A. C., Mitchell, M., Yuan, F., & Ruhland, C. T. (2019). Intensification of midwestern agriculture as a regional climate modifier and atmospheric boundary layer moisture source. *Annals of the Association of American Geographers*, *109*(6), 1–20. https://doi.org/10.1080/24694452.2019.1598842

Hill, A. C., Vázquez-Lule, A., & Vargas, R. (2021). Linking vegetation spectral reflectance with ecosystem carbon phenology in a temperate salt marsh. *Agricultural and Forest Meteorology*, *307*, 108481. https://doi.org/10.1016/j.agrformet.2021.108481

Holm, G. O., Perez, B. C., McWhorter, D. E., Krauss, K. W., Johnson, D. J., Raynie, R. C., & Killebrew, C. J. (2016). Ecosystem level methane fluxes from tidal freshwater and brackish marshes of the Mississippi river delta: Implications for coastal wetland carbon projects. *Wetlands*, *36*(3), 401–413. https://doi.org/10.1007/s13157-016-0746-7

Holmquist, J. R., Brown, L. N., & MacDonald, G. M. (2021). Localized scenarios and latitudinal patterns of vertical and lateral resilience of tidal marshes to sea-level rise in the contiguous United States. *Earth's Future*, *9*(6). https://doi.org/10.1029/2020ef001804

Holmquist, J. R., & Windham-Myers, L. (2022). A conterminous USA-scale map of relative tidal marsh elevation. *Estuaries and Coasts*. https://doi.org/10.1007/s12237-021-01027-9

Huang, J. F., Luo, M., Liu, Y. X., Zhang, Y. X., & Tan, J. (2019). Effects of tidal scenarios on the methane emission dynamics in the subtropical tidal marshes of the min river Estuary in Southeast China. *International Journal of Environmental Research and Public Health*, *16*(15), 2790. https://doi.org/10.3390/ijerph16152790

Huang, Y., Chen, Z. H., Tian, B., Zhou, C., Wang, J. T., Ge, Z. M., & Tang, J. W. (2020). Tidal effects on ecosystem CO_2 exchange in a Phragmites salt marsh of an intertidal shoal. *Agricultural and Forest Meteorology*, *292*, 108108. https://doi.org/10.1016/j.agrformet.2020.108108

Huertas, I. E., de la Paz, M., Perez, F. F., Navarro, G., & Flecha, S. (2019). Methane emissions from the salt marshes of Donana wetlands: Spatio-temporal variability and controlling factors. *Frontiers in Ecology and Evolution*, *7*. https://doi.org/10.3389/fevo.2019.00032

Janssens, I. A., Kowalski, A. S., Longdoz, B., & Ceulemans, R. (2000). Assessing forest soil CO_2 efflux: An in situ comparison of four techniques. *Tree Physiology*, *20*(1), 23–32. https://doi.org/10.1093/treephys/20.1.23

Kathilankal, J. C., Mozdzer, T. J., Fuentes, J. D., D'Odorico, P., McGlathery, K. J., & Zieman, J. C. (2008). Tidal influences on carbon assimilation by a salt marsh. *Environmental Research Letters*, *3*(4), 044010. https://doi.org/10.1088/1748-9326/3/4/044010

Kathilankal, J. C., Mozdzer, T. J., Fuentes, J. D., McGlathery, K. J., D'Odorico, P., & Zieman, J. C. (2011). Physiological responses of Spartina alterniflora to varying environmental conditions in Virginia marshes. *Hydrobiologia*, *669*(1), 167–181. https://doi.org/10.1007/s10750-011-0681-9

Kennish, M. J. (2019). The national estuarine research Reserve system: A review of research and monitoring initiatives. *Open Journal of Ecology*, *9*(3), 50–65. https://doi.org/10.4236/oje.2019.93006

Kirwan, M. L., & Megonigal, J. P. (2013). Tidal wetland stability in the face of human impacts and sea-level rise. *Nature*, *504*(7478), 53–60. https://doi.org/10.1038/nature12856

Kirwan, M. L., Temmerman, S., Skeehan, E. E., Guntenspergen, G. R., & Fagherazzi, S. (2016). Overestimation of marsh vulnerability to sea level rise. *Nature Climate Change*, *6*(3), 253–260. https://doi.org/10.1038/nclimate2909

Knox, S. H., Bansal, S., McNicol, G., Schafer, K., Sturtevant, C., Ueyama, M., et al. (2021). Identifying dominant environmental predictors of freshwater wetland methane fluxes across diurnal to seasonal time scales. *Global Change Biology*, *27*(15), 3582–3604. https://doi.org/10.1111/gcb.15661

Knox, S. H., Windham-Myers, L., Anderson, F., Sturtevant, C., & Bergamaschi, B. (2018). Direct and indirect effects of tides on ecosystem-scale CO_2 exchange in a brackish tidal marsh in northern California. *Journal of Geophysical Research: Biogeosciences*, *123*(3), 787–806. https://doi.org/10.1002/2017jg004048

Komsta, L., & Novomestky, F. (2015). *Moments, cumulants, skewness, kurtosis and related tests* (p. 14). R package version.

Kormann, R., & Meixner, F. X. (2001). An analytical footprint model for non-neutral stratification. *Boundary-Layer Meteorology*, *99*(2), 207–224. https://doi.org/10.1023/A:1018991015119

Kostka, J. E., Roychoudhury, A., & Van Cappellen, P. (2002). Rates and controls of anaerobic microbial respiration across spatial and temporal gradients in saltmarsh sediments. *Biogeochemistry*, *60*(1), 49–76. https://doi.org/10.1023/a:1016525216426

Krauss, K. W., Holm, G. O., Perez, B. C., McWhorter, D. E., Cormier, N., Moss, R. F., et al. (2016). Component greenhouse gas fluxes and radiative balance from two deltaic marshes in Louisiana: Pairing chamber techniques and eddy covariance. *Journal of Geophysical Research: Biogeosciences*, *121*(6), 1503–1521. https://doi.org/10.1002/2015jg003224

Lamers, L. P. M., Govers, L. L., Janssen, I., Geurts, J. J. M., Van der Welle, M. E. W., Van Katwijk, M. M., et al. (2013). Sulfide as a soil phytotoxin: A review. *Frontiers of Plant Science*, *4*. https://doi.org/10.3389/fpls.2013.00268

Lasslop, G., Migliavacca, M., Bohrer, G., Reichstein, M., Bahn, M., Ibrom, A., et al. (2012). On the choice of the driving temperature for eddy-covariance carbon dioxide flux partitioning. *Biogeosciences*, *9*(12), 5243–5259. https://doi.org/10.5194/bg-9-5243-2012

Lees, K. J., Khomik, M., Quaife, T., Clark, J. M., Hill, T., Klein, D., & Artz, R. R. E. (2021). Assessing the reliability of peatland GPP measurements by remote sensing: From plot to landscape scale. *Science of the Total Environment*, 766. 142613. https://doi.org/10.1016/j.scitotenv.2020.142613

Li, H., Dai, S., Ouyang, Z., Xie, X., Guo, H., Gu, C., et al. (2018). Multi-scale temporal variation of methane flux and its controls in a subtropical tidal salt marsh in eastern China. *Biogeochemistry*, *137*(1), 163–179. https://doi.org/10.1007/s10533-017-0413-y

Limmer, M. A., Mann, J., Amaral, D. C., Vargas, R., & Seyfferth, A. L. (2018). Silicon-rich amendments in rice paddies: Effects on arsenic uptake and biogeochemistry. *Science of the Total Environment*, *624*, 1360–1368. https://doi.org/10.1016/j.scitotenv.2017.12.207

Liu, L. J., Wang, D. Q., Chen, S., Yu, Z. J., Xu, Y. K., Li, Y., et al. (2019). Methane emissions from estuarine coastal wetlands: Implications for global change effect. *Soil Science Society of America Journal*, *83*(5), 1368–1377. https://doi.org/10.2136/sssaj2018.12.0472

Lu, W., Xiao, J., Liu, F., Zhang, Y., Liu, C. a., & Lin, G. (2017). Contrasting ecosystem CO_2 fluxes of inland and coastal wetlands: A meta-analysis of eddy covariance data. *Global Change Biology*, *23*(3), 1180–1198. https://doi.org/10.1111/gcb.13424

Lucas-Moffat, A. M., Huth, V., Augustin, J., Brummer, C., Herbst, M., & Kutsch, W. L. (2018). Towards pairing plot and field scale measurements in managed ecosystems: Using eddy covariance to cross-validate CO_2 fluxes modeled from manual chamber campaigns. *Agricultural and Forest Meteorology*, *256*, 362–378. https://doi.org/10.1016/j.agrformet.2018.01.023

McKenna, T., Callahan, J., Medlock, C., & Bates, N. (2018). Creation of improved accuracy LiDAR-based digital elevation models for the St. Jones river and Blackbird creek watersheds. *Newark: Delaware Geologic Survey, Technical Report*, 1–30.

Megonigal, J. P., & Guenther, A. B. (2008). Methane emissions from upland forest soils and vegetation. *Tree Physiology*, *28*(4), 491–498. https://doi.org/10.1093/treephys/28.4.491

Meijide, A., Manca, G., Goded, I., Magliulo, V., di Tommasi, P., Seufert, G., & Cescatti, A. (2011). Seasonal trends and environmental controls of methane emissions in a rice paddy field in Northern Italy. *Biogeosciences*, *8*(12), 3809–3821. https://doi.org/10.5194/bg-8-3809-2011

Mitra, B., Minick, K., Miao, G., Domec, J.-C., Prajapati, P., McNulty, S. G., et al. (2020). Spectral evidence for substrate availability rather than environmental control of methane emissions from a coastal forested wetland. *Agricultural and Forest Meteorology*, *291*, 108062. https://doi.org/10.1016/j.agrformet.2020.108062

Moffett, K. B., & Gorelick, S. M. (2016). Relating salt marsh pore water geochemistry patterns to vegetation zones and hydrologic influences. *Water Resources Research*, *52*(3), 1729–1745. https://doi.org/10.1002/2015wr017406

Moncrieff, J., Clement, R., Finnigan, J., & Meyers, T. (2005). Averaging, detrending, and filtering of eddy covariance time series. In X. Lee, W. Massman, & B. Law (Eds.), *Handbook of micrometeorology: A guide for surface flux measurement and analysis* (pp. 7–31). Springer Netherlands. https://doi.org/10.1007/1-4020-2265-4_2

Morin, T. H., Bohrer, G., Naor-Azrieli, L., Mesi, S., Kenny, W. T., Mitsch, W. J., & Schafer, K. V. R. (2014). The seasonal and diurnal dynamics of methane flux at a created urban wetland. *Ecological Engineering*, *72*, 74–83. https://doi.org/10.1016/j.ecoleng.2014.02.002

Morin, T. H., Bohrer, G., Stefanik, K. C., Rey-Sanchez, A. C., Matheny, A. M., & Mitsch, W. J. (2017). Combining eddy-covariance and chamber measurements to determine the methane budget from a small, heterogeneous urban floodplain wetland park. *Agricultural and Forest Meteorology*, *237*, 160–170. https://doi.org/10.1016/j.agrformet.2017.01.022

Nahrawi, H., Leclerc, M., Pennings, S., Zhang, G., Singh, N., & Pahari, R. (2020). Impact of tidal inundation on the net ecosystem exchange in daytime conditions in a salt marsh. *Agricultural and Forest Meteorology*, *294*, 108133. https://doi.org/10.1016/j.agrformet.2020.108133

Oertel, C., Matschullat, J., Zurba, K., Zimmermann, F., & Erasmi, S. (2016). Greenhouse gas emissions from soils A review. *Chemie Der Erde-Geochemistry*, *76*(3), 327–352. https://doi.org/10.1016/j.chemer.2016.04.002

Olsson, L., Ye, S., Yu, X., Wei, M., Krauss, K. W., & Brix, H. (2015). Factors influencing CO_2 and CH_4 emissions from coastal wetlands in the Liaohe Delta, Northeast China. *Biogeosciences*, *12*(16), 4965–4977. https://doi.org/10.5194/bg-12-4965-2015

Pearson, A. J., Pizzuto, J. E., & Vargas, R. (2016). Influence of run of river dams on floodplain sediments and carbon dynamics. *Geoderma*, *272*, 51–63. https://doi.org/10.1016/j.geoderma.2016.02.029

Peterson, P. M., Romaschenko, K., Arrieta, Y. H., & Saarela, J. M. (2014). A molecular phylogeny and new subgeneric classification of Sporobolus (Poaceae: Chloridoideae: Sporobolinae). *Taxon*, *63*(6), 1212–1243. https://doi.org/10.12705/636.19

Pezeshki, S. R. (2001). Wetland plant responses to soil flooding. *Environmental and Experimental Botany*, *46*(3), 299–312. https://doi.org/10.1016/s0098-8472(01)00107-1

Phillips, C. L., Bond-Lamberty, B., Desai, A. R., Lavoie, M., Risk, D., Tang, J. W., et al. (2017). The value of soil respiration measurements for interpreting and modeling terrestrial carbon cycling. *Plant and Soil*, *413*(1–2), 1–25. https://doi.org/10.1007/s11104-016-3084-x

Pinheiro, J., Bates, D., DebRoy, S., Sarkar, D., Heisterkamp, S., Van Willigen, B., & Maintainer, R. (2017). Package 'nlme'. *Linear and nonlinear mixed effects models, version*, *3*(1).

Poffenbarger, H. J., Needelman, B. A., & Megonigal, J. P. (2011). Salinity influence on methane emissions from tidal marshes. *Wetlands*, *31*(5), 831–842. https://doi.org/10.1007/s13157-011-0197-0

Poyda, A., Reinsch, T., Skinner, R. H., Kluß, C., Loges, R., & Taube, F. (2017). Comparing chamber and eddy covariance based net ecosystem CO_2 exchange of fen soils. *Journal of Plant Nutrition and Soil Science*, *180*(2), 252–266. https://doi.org/10.1002/jpln.201600447

R Core Team. (2020). *R: A language and environment for statistical computing*. R Foundation for Statistical Computing. https://www.R-project.org/

Reichstein, M., Falge, E., Baldocchi, D., Papale, D., Aubinet, M., Berbigier, P., et al. (2005). On the separation of net ecosystem exchange into assimilation and ecosystem respiration: Review and improved algorithm. *Global Change Biology*, *11*(9), 1424–1439. https://doi.org/10.1111/j.1365-2486.2005.001002.x

Reichstein, M., Stoy, P. C., Desai, A. R., Lasslop, G., & Richardson, A. D. (2012). *Partitioning of net fluxes Eddy covariance* (pp. 263–289). Springer. https://doi.org/10.1007/978-94-007-2351-1_9

Rey-Sanchez, A. C., Morin, T. H., Stefanik, K. C., Wrighton, K., & Bohrer, G. (2018). Determining total emissions and environmental drivers of methane flux in a Lake Erie estuarine marsh. *Ecological Engineering*, *114*, 7–15. https://doi.org/10.1016/j.ecoleng.2017.06.042

Riederer, M., Serafimovich, A., & Foken, T. (2014). Net ecosystem CO_2 exchange measurements by the closed chamber method and the eddy covariance technique and their dependence on atmospheric conditions. *Atmospheric Measurement Techniques*, *7*(4), 1057–1064. https://doi.org/10.5194/amt-7-1057-2014

Schafer, K. V. R., Tripathee, R., Artigas, F., Morin, T. H., & Bohrer, G. (2014). Carbon dioxide fluxes of an urban tidal marsh in the Hudson-Raritan estuary. *Journal of Geophysical Research: Biogeosciences*, *119*(11), 2065–2081. https://doi.org/10.1002/2014jg002703

Seyfferth, A. L., Bothfeld, F., Vargas, R., Stuckey, J. W., Wang, J., Kearns, K., et al. (2020). Spatial and temporal heterogeneity of geochemical controls on carbon cycling in a tidal salt marsh. *Geochimica et Cosmochimica Acta*, *282*, 1–18. https://doi.org/10.1016/j.gca.2020.05.013

Stoy, P. C., Katul, G. G., Siqueira, M. B. S., Juang, J.-Y., Novick, K. A., Uebelherr, J. M., & Oren, R. (2006). An evaluation of models for partitioning eddy covariance-measured net ecosystem exchange into photosynthesis and respiration. *Agricultural and Forest Meteorology*, *141*(1), 2–18. https://doi.org/10.1016/j.agrformet.2006.09.001

Sun, L., Song, C. C., Miao, Y. Q., Qiao, T. H., & Gong, C. (2013). Temporal and spatial variability of methane emissions in a northern temperate marsh. *Atmospheric Environment*, *81*, 356–363. https://doi.org/10.1016/j.atmosenv.2013.09.033

Thottathil, S. D., Reis, P. C. J., & Prairie, Y. T. (2019). Methane oxidation kinetics in northern freshwater lakes. *Biogeochemistry*, *143*(1), 105–116. https://doi.org/10.1007/s10533-019-00552-x

Tobias, C., & Neubauer, S. C. (2019). Chapter 16 - salt marsh biogeochemistry—An overview. In G. M. E. Perillo, E. Wolanski, D. R. Cahoon, & C. S. Hopkinson (Eds.), *Coastal wetlands* (pp. 539–596). Elsevier. https://doi.org/10.1016/B978-0-444-63893-9.00016-2

Tong, C., Wang, W. Q., Zeng, C. S., & Marrs, R. (2010). Methane (CH_4) emission from a tidal marsh in the Min River estuary, southeast China. *Journal of Environmental Science and Health—Part A: Toxic/Hazardous Substances & Environmental Engineering*, *45*(4), 506–516. https://doi.org/10.1080/10934520903542261

Trifunovic, B., Vazquez-Lule, A., Capooci, M., Seyfferth, A. L., Moffat, C., & Vargas, R. (2020). Carbon dioxide and methane emissions from temperate salt marsh tidal creek. *Journal of Geophysical Research: Biogeosciences*, *125*(8). https://doi.org/10.1029/2019jg005558

Vazquez-Lule, A., & Vargas, R. (2021). Biophysical drivers of net ecosystem and methane exchange across phenological phases in a tidal salt marsh. *Agricultural and Forest Meteorology*, *300*, 108309. https://doi.org/10.1016/j.agrformet.2020.108309

Villa, J. A., Ju, Y., Yazbeck, T., Waldo, S., Wrighton, K. C., & Bohrer, G. (2021). Ebullition dominates methane fluxes from the water surface across different ecohydrological patches in a temperate freshwater marsh at the end of the growing season. *Science of the Total Environment*, *767*, 144498. https://doi.org/10.1016/j.scitotenv.2020.144498

Wang, F. M., Sanders, C. J., Santos, I. R., Tang, J. W., Schuerch, M., Kirwan, M. L., et al. (2021). Global blue carbon accumulation in tidal wetlands increases with climate change. *National Science Review*, *8*(9). https://doi.org/10.1093/nsr/nwaa296

Wang, M., Guan, D. X., Han, S. J., & Wu, J. L. (2010). Comparison of eddy covariance and chamber-based methods for measuring CO_2 flux in a temperate mixed forest. *Tree Physiology*, *30*(1), 149–163. https://doi.org/10.1093/treephys/tpp098

Warner, D. L., Vargas, R., Seyfferth, A., & Inamdar, S. (2018). Transitional slopes act as hotspots of both soil CO_2 emission and CH_4 uptake in a temperate forest landscape. *Biogeochemistry*, *138*(2), 121–135. https://doi.org/10.1007/s10533-018-0435-0

Wei, S. Y., Han, G. X., Jia, X., Song, W. M., Chu, X. J., He, W. J., et al. (2020). Tidal effects on ecosystem CO_2 exchange at multiple timescales in a salt marsh in the Yellow River Delta. *Estuarine, Coastal and Shelf Science*, *238*, 106727. https://doi.org/10.1016/j.ecss.2020.106727

Wutzler, T., Lucas-Moffat, A., Migliavacca, M., Knauer, J., Sickel, K., Šigut, L., et al. (2018). Basic and extensible post-processing of eddy covariance flux data with REddyProc. *Biogeosciences*, *15*(16), 5015–5030. https://doi.org/10.5194/bg-15-5015-2018

Xu, X. W., Zou, X. Q., Cao, L. G., Zhamangulova, N., Zhao, Y. F., Tang, D. H., & Liu, D. W. (2014). Seasonal and spatial dynamics of greenhouse gas emissions under various vegetation covers in a coastal saline wetland in southeast China. *Ecological Engineering*, *73*, 469–477. https://doi.org/10.1016/j.ecoleng.2014.09.087

Yang, B., Li, X., Lin, S., Jiang, C., Xue, L., Wang, J., et al. (2021). Invasive Spartina alterniflora changes the Yangtze Estuary salt marsh from CH_4 sink to source. *Estuarine, Coastal and Shelf Science*, *252*, 107258. https://doi.org/10.1016/j.ecss.2021.107258

Yang, P., Lai, D. Y. F., Huang, J. F., Zhang, L. H., & Tong, C. (2018). Temporal variations and temperature sensitivity of ecosystem respiration in three brackish marsh communities in the Min River Estuary, southeast China. *Geoderma*, *327*, 138–150. https://doi.org/10.1016/j.geoderma.2018.05.005

Ye, Z.-P., Ling, Y., Yu, Q., Duan, H.-L., Kang, H.-J., Huang, G.-M., et al. (2020). Quantifying light response of leaf-scale water-use efficiency and its interrelationships with photosynthesis and stomatal conductance in C3 and C4 species. *Frontiers of Plant Science*, *11*. https://doi.org/10.3389/fpls.2020.00374

You, Y., Staebler, R. M., Moussa, S. G., Beck, J., & Mittermeier, R. L. (2021). Methane emissions from an oil sands tailings pond: A quantitative comparison of fluxes derived by different methods. *Atmospheric Measurement Techniques*, *14*(3), 1879–1892. https://doi.org/10.5194/amt-14-1879-2021

Yu, L. F., Wang, H., Wang, G. S., Song, W. M., Huang, Y., Li, S. G., et al. (2013). A comparison of methane emission measurements using eddy covariance and manual and automated chamber-based techniques in Tibetan Plateau alpine wetland. *Environmental Pollution*, *181*, 81–90. https://doi.org/10.1016/j.envpol.2013.06.018